Quantum Turbulence

Makoto Tsubota[1 * †]
[1]Department of Physics, Osaka City University, Japan

The present article reviews the recent developments in the physics of quantum hydrodynamics and quantum turbulence in superfluid helium and atomic Bose-Einstein condensates. Quantum turbulence (QT) was discovered in superfluid ^{4}He in the 1950s, and the research has tended toward a new direction since the mid 1990s. QT is comprised of quantized vortices that are definite topological defects, being expected to yield a model of turbulence that is much simpler than the classical model. The general introduction of the issue and a brief review on classical turbulence are followed by a description of the dynamics of quantized vortices. The first modern topic is a vortex lattice formation in a rotating Bose-Einstein condensate. The second describes the modern trends on quantum turbulence in superfluid helium, addressing the energy spectrum of QT, the possible dissipation mechanism at very low temperatures, temperature-dependent transition to QT, QT created by vibrating structures, and visualization of QT. The last topic is QT in atomic Bose-Einstein condensates.

Keywords: Quantum turbulence, Quantized vortex, Superfluid, Bose-Einstein condensation

1. INTRODUCTION

Nature is filled with fluid flow, from small scales to large scales. Our daily life on a human scale constantly experiences currents of air, water, and the like. The earth sustains the ocean flows and atmospheric circulation, leading to an abundance of life. In space, stars and galaxies flow, forming many large-scale structures. Most flow in nature is actually turbulent. As the velocity increases, flow generally changes from laminar to turbulent. For high-velocity or high Reynolds number flows, the flow is generally turbulent. Turbulence has been investigated not only in basic science research, such as physics and mathematics research, but also in applied sciences, such as fluid engineering and aeronautics, while it is still not yet well understood. As Feynman said, turbulence is a problem "that is common to many fields, that is very old, and that has not been solved." [1] This is chiefly because turbulence is a complicated dynamical phenomenon with strong nonlinearity that is quite different from an equilibrium state.

"Turbulence" reminds one of some sketches by Leonardo da Vinci. He observed the turbulent flow of water and drew pictures showing that turbulence has a structure comprised of vortices of different sizes (Fig. 1). Vortices may be a key to understanding turbulence. However, vortices are not well defined for a typical classical fluid, and the relationship between turbulence and vortices remains unclear.

Independently of these studies in classical fluid dynamics, quantum fluids such as superfluid helium and atomic Bose-Einstein condensates (BECs) have been investigated in the field of low temperature physics. These systems are subject to severe quantum restrictions; the appearance of order parameters makes the rotational motion exist only in the presence of quantized vortices. A quantized vortex is a stable topological defect with quantized circulation. Such vortices give rise to quantum turbulence (QT). Since quantized vortices are well defined as elements composing a turbulent flow, QT is expected to be an easier system to study than classical turbulence (CT) and has a simpler model of turbulence.

This article reviews recent developments in quantum hydrodynamics and QT in superfluid helium and atomic BECs. In Sec. 2, basic concepts such as superfluidity, Bose-Einstein condensation, and quantized vortices are briefly reviewed. Section 3 is devoted to statistical properties of CT, and the comparison between CT and QT. Section 4 addresses the general description of dynamics of quantized vortices. In

*E-mail: tsubota@sci.osaka-cu.ac.jp
†Present address: Department of Physics, Osaka City University, Osaka 558–8585, Japan.

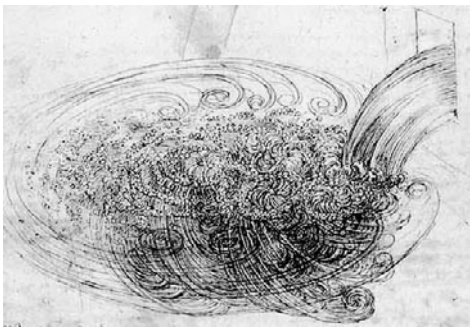

Fig. 1. Sketch of turbulence by da Vinci.

Sec.5 we discuss the dynamics of vortex lattice formation in a rotating BEC, addressing typical phenomena of quantum hydrodynamics. Section 6 describes present important topics of QT in superfluid helium, involving the energy spectrum of QT, the possible dissipation mechanism at very low temperatures, temperature-dependent transition to QT, QT created by vibrating structures, and visualization of QT. Applying these ideas, QT in atomic BECs is finally discussed in Sec. 7. Section 8 is devoted to conclusions.

2. BOSE-EINSTEIN CONDENSATION, SUPERFLUIDITY, AND QUANTIZED VORTICES

This section reviews briefly the backgrounds of low temperature physics necessary for understanding this article.

2.1 Bose-Einstein Condensation

Quantum mechanics, which has developed since the beginning of the 20th century, has changed drastically our natural philosophy. Quantum mechanics is often thought to give the physical laws at microscopic scales, but this understanding is not necessarily correct. Quantum mechanics actually obeys the physical laws even at macroscopic scales. Such a field is quantum statistical mechanics.

The essence of quantum mechanics is the duality of particle-picture and wave-picture. Let's consider an ideal atomic gas. At relatively high temperatures, the statistics of the atoms obeys the classical Maxwell-Boltzman distribution and each atom behaves like a particle. As the temperature is reduced, however, the thermal de Broglie wavelength is increased to become comparable to the mean distance between atoms. Then each atom becomes to behave like a wave, and the statistics changes to the quantum Fermi-Dirac or Bose-Einstein distribution depending on whether the atom is a Fermion or a Boson. If the atoms are Bosons and the system is cooled below a critical temperature T_{BEC}, they cause Bose-Einstein condensation in which these atoms occupy the same single-particle ground state[2]; the critical temperature is given by

$$T_{\mathrm{BEC}} = 3.3 \frac{\hbar^2 n^{2/3}}{m k_B}, \tag{1}$$

where the relevant quantities are the particle mass m, the number density n, the Planck constant $h = 2\pi\hbar$, and the Boltzman constant k_B. Then matter-waves of atoms become coherent to make a macroscopic wave function (the order parameter) $\Psi(\mathrm{x}, t) = |\Psi(\mathrm{x}, t)|e^{i\theta(\mathrm{x},t)}$ extending over the whole volume of the system, and the assemblage of these atoms is called a Bose-Einstein condensate (BEC). Thus quantum mechanics appears at macroscopic scales through Bose-Einstein condensation.

Bose-Einstein condensation was theoretically predicted by Einstein in 1925. However, nobody knew in those days a system in which Bose-Einstein condensation occurs actually.

2.2 Liquid Helium and Superfluidity

Independently of these studies in quantum statistical mechanics, the field of low temperature physics has developed since the beginning of 20th century. Low temperature physics is generally believed to start with the first liquefaction of ^{4}He at 4.2K by Onnes in 1908. Subsequently, Onnes observed

superconductivity in mercury in 1911. Onnes noticed the anomaly of heat capacity of liquid helium at the λ point T_λ= 2.17 K too [1]. In 1938 Kapitza *et al*. observed that liquid ^{4}He becomes inviscid below the λ point and called this striking phenomenon *superfluidity* [3].

London proposed theoretically in 1938 that the λ transition is caused by Bose-Einstein condensation of ^{4}He atoms. When $T_{\rm BEC}$ of Eq. (1) is evaluated for the mass and density appropriate to liquid ^{4}He at saturated vapor pressure, one obtains $T_{\rm BEC}$ of approximately 3.13K, which is close to T_λ = 2.17 K[2].

2.3 Two-Fluid Model and a Quantized Vortex

In order to explain various hydrodaynamic phenomena of superfluidity[3], Tisza and Landau introduced the two-fluid model. According to the two-fluid model, the system consists of an inviscid superfluid (density ρ_s) and a viscous normal fluid (density ρ_n) with two independent velocity fields $\mathbf{v}_s$ and $\mathbf{v}_n$. The mixing ratio of the two fluids depends on temperature. As the temperature is reduced below the λ point, the ratio of the superfluid component increases, and the entire fluid becomes a superfluid below approximately 1 K. The Bose-condensed system exhibits the macroscopic wave function $\Psi(\mathbf{x}, t) = |\Psi(\mathbf{x}, t)|e^{i\theta(\mathrm{x},t)}$ as an order parameter. The superfluid velocity field is given by $\mathbf{v}_s = (\hbar/m)\nabla\theta$ with boson mass m, representing the potential flow. Since the macroscopic wave function should be single-valued for the space coordinate $\mathbf{x}$, the circulation $\mathrm{T} = \oint \mathbf{v} \cdot d\ell$ for an arbitrary closed loop in the fluid is quantized by the quantum $k = h/m$. A vortex with such quantized circulation is called a quantized vortex. Any rotational motion of a superfluid is sustained only by quantized vortices. A quantized vortex was predicted by Feynman [4] and observed experimentally in helium by Vinen [5].

A quantized vortex is a topological defect characteristic of a Bose-Einstein condensate and is different from a vortex in a classical viscous fluid. First, the circulation is quantized, which is contrary to a classical vortex that can have any value of circulation. Second, a quantized vortex is a vortex of inviscid superflow. Thus, it cannot decay by the viscous diffusion of vorticity that occurs in a classical fluid. Third, the core of a quantized vortex is very thin, on the order of the coherence length, which is only a few angstroms in superfluid ^{4}He. Since the vortex core is very thin and does not decay by diffusion, it is always possible to identify the position of a quantized vortex in the fluid. These properties make a quantized vortex more stable and definite than a classical vortex.

2.4 Early Studies on Superfluid Tubrulence

Early experimental studies on superfluid turbulence focused primarily on thermal counterflow, in which the normal fluid and superfluid flow in opposite directions. The flow is driven by an injected heat current, and it was found that the superflow becomes dissipative when the relative velocity between the two fluids exceeds a critical value [6]. Feynman proposed that this is a superfluid turbulent state consisting of a tangle of quantized vortices [4]. Vinen later confirmed Feynman's findings experimentally by showing that the dissipation comes from the mutual friction between vortices and the normal flow [7, 8, 9, 10]. Subsequently, several experimental studies have examined superfluid turbulence (ST) in thermal counterflow systems and have revealed a variety of physical phenomenon[11]. Since the dynamics of quantized vortices is nonlinear and non-local, it has not been easy to understand vortex dynamics observations quantitatively. Schwarz clarified the picture of ST consisting of tangled vortices by a numerical simulation of the quantized vortex filament model in the thermal counterflow [12, 13]. However, since the thermal counterflow has no analogy to conventional fluid dynamics, this study was not helpful in clarifying the relationship between ST and classical turbulence (CT). Superfluid turbulence is often called quantum turbulence (QT), which emphasizes the fact that it is comprised of quantized vortices.

3. CLASSICAL TURBULENCE AND QUANTUM TURBULENCE

Before considering QT, we briefly review classical fluid dynamics and the statistical properties of CT [14], then compare CT and QT.

---

[1]Since the curve of the temperature dependence of the heat capacity resembles a Greek letter λ, the critical temperature 2.17K is called the λ point or the λ temperature. The superfluid transition of liquid ^{4}He at 2.17 K is called the λ transition.

[2]Landau criticized London for this idea. Liquid helium has weak interatomic interaction, and is not an ideal Bose gas. Hence the application of Eq. (1) is not exactly correct The inelastic neutron scattering experiments in 1980s observed the presence of the BEC below the λ point, and it is now understood that the λ transition is caused by Bose-Einstein condensation. However, the interaction depresses the condensates compared to the case of an ideal gas.

3.1 Statistical Properties of Classical Turbulence

Classical viscous fluid dynamics is described by the Navier–Stokes equation:

$$\frac{\partial}{\partial t}\mathbf{v}(\mathbf{x}, t) + \mathbf{v}(\mathbf{x}, t) \cdot \nabla \mathbf{v}(\mathbf{x}, t) = -\frac{1}{\rho}\nabla P(\mathbf{x}, t) + \nu \nabla^2 \mathbf{v}(\mathbf{x}, t), \tag{2}$$

where $\mathbf{v}(\mathbf{x}, t)$ is the velocity of the fluid, $P(\mathbf{x}, t)$ is the pressure, ρ is the density of the fluid, and ν is the kinematic viscosity. The flow of this fluid can be characterized by the ratio of the second term of the left-hand side of Eq. (2), hereinafter referred to as the inertial term, to the second term of the right-hand side, hereinafter called the viscous term. This ratio is the Reynolds number $R = \bar{\upsilon}D/\nu$, where $\bar{\upsilon}$ and D are the characteristic velocity of the flow and the characteristic scale, respectively. When $\bar{\upsilon}$ increases to allow the Reynolds number to exceed a critical value, the system changes from a laminar state to a turbulent state, in which the flow is highly complicated and contains many eddies.

Such turbulent flow is known to show characteristic statistical behavior [15, 16]. We assume a steady state of fully developed turbulence of an incompressible classical fluid. The energy is injected into the fluid at a rate of ε, the scale of which is comparable to the system size D in the energy-containing range. In the inertial range, this energy is transferred to smaller scales without being dissipated. In this range, the system is locally homogeneous and isotropic, which leads to the statistics of the energy spectrum known as the Kolmogorov law:

$$E(k) = C\, \varepsilon^{2/3} k^{-5/3}. \tag{3}$$

Here, the energy spectrum $E(k)$ is defined as $E = \int d\mathbf{k} E(k)$, where E is the kinetic energy per unit mass and k is the wavenumber from the Fourier transformation of the velocity field. The spectrum of Eq. (3) is easily derived by assuming that $E(k)$ is locally determined by only the energy flux ε and k. The energy transferred to smaller scales in the energy-dissipative range is dissipated at the Kolmogorov wavenumber $k_K = (\in/\nu^3)^{1/4}$ through the viscosity of the fluid with dissipation rate ε in Eq. (3), which is equal to the energy flux Π in the inertial range. The Kolmogorov constant C is a dimensionless parameter of order unity. The Kolmogorov spectrum is confirmed experimentally and numerically in turbulence at high Reynolds numbers. The inertial range is thought to be sustained by the self-similar Richardson cascade in which large eddies are broken up into smaller eddies through many vortex reconnections. In CT, however, the Richardson cascade is not completely understood because it is impossible to definitely identify each eddy. The Kolmogorov spectrum is based on the assumption that the turbulence is homogeneous and isotropic. However, actual turbulence is not necessarily homogeneous or isotropic, and so the energy spectrum deviates from the Kolmogorov form. This phenomenon is called intermittency, and is an important problem in modern fluid dynamics [14]. Intermittency is closely related to the coherent structure, which may be represented by vortices. Research into QT could also shed light on this issue.

3.2 Classical Turbulence and Quantum Turbulence

Comparing QT and CT reveals definite differences. Turbulence in a classical viscous fluid appears to be comprised of vortices, as pointed out by da Vinci. However, these vortices are unstable, repeatedly appearing and disappearing. Moreover, the circulation is not conserved and is not identical for each vortex. Quantum turbulence consists of a tangle of quantized vortices that have the same conserved circulation. Looking back at the history of science, *reductionism*, which tries to understand the nature of complex things by reducing them to the interactions of their parts, has played an extremely important role. The success of solid state physics owes much to *reductionism*. In contrast, conventional fluid physics is not reducible to elements, and thus does not enjoy the benefits of *reductionism*. However, quantum turbulence is different, being reduced to quantized vortices. Thus *reductionism* is applicable to quantum turbulence. Consequently, QT should lead to a simpler model of turbulence than CT.

3.3 Research Trends of Quantum Hydrodynamics

Based on these considerations, research into quantum hydrodynamics has opened up new directions since the mid 1990s. One new direction has occurred in the field of low temperature physics by studying superfluid helium. It started with the attempt to understand the relationship between QT and CT [17, 18]. Recent experimental and numerical studies support a Kolmogorov spectrum in QT.

Following these studies, QT research on superfluid helium has moved to important topics such as the dissipation process at very low temperatures, QT created by vibrating structures, and visualization of QT [19, 20, 21]. Another new direction is the realization of Bose-Einstein condensation in trapped atomic gases in 1995, which has stimulated intense experimental and theoretical activity [2]. As proof of the existence of superfluidity, quantized vortices have been created and observed in atomic BECs, and numerous efforts have been devoted to a number of fascinating problems [22]. Atomic BECs have several advantages over superfluid helium. The most important is that modern optical techniques enable one to directly control condensates and visualize quantized vortices. A series of experiments on BECs clearly show the properties of quantum hydrodynamics [23, 24, 25].

4. DYNAMICS OF QUANTIZED VORTICES

Quantum hydrodynamics is reduced to the dynamics of quantized vortices as elements, which is addressed in this section. As described in Section 2, most experimental studies on superfluid turbulence have examined thermal counterflow. However, the nonlinear and non-local dynamics of vortices have delayed progress in the microscopic understanding of the vortex tangle. Schwarz overcame these difficulties [12, 13] by developing a direct numerical simulation of vortex dynamics connected with dynamical scaling analysis, enabling the calculation of physical quantities such as the vortex line density, anisotropic parameters, and mutual friction force. The observable quantities obtained by Schwarz agree well with some typical experimental results.

Two formulations are generally available for studying the dynamics of quantized vortices. One is the vortex filament model and the other is the Gross-Pitaevskii (GP) model. We will briefly review these two formulations.

4.1 Vortex Filament Model

As described in Section 2, a quantized vortex has quantized circulation. The vortex core is extremely thin, usually much smaller than other characteristic scales in vortex motion. The vortex core is supposed to be hollow, there are no direct observations in helium though. These properties allow a quantized vortex to be represented as a vortex filament. In classical fluid dynamics [26], the vortex filament model is a convenient idealization. However, the vortex filament model is accurate and realistic for a quantized vortex in superfluid helium.

The vortex filament formulation represents a quantized vortex as a filament passing through the fluid, having a definite direction corresponding to its vorticity. Except for the thin core region, the superflow velocity field has a classically well-defined meaning and can be described by ideal fluid dynamics. The velocity at a point $\mathbf{r}$ due to a filament is given by the Biot-Savart expression:

$$\mathbf{v}_s(\mathbf{r}) = \frac{\kappa}{4\pi}\int_{\mathcal{L}} \frac{(\mathbf{s}_1 - \mathbf{r}) \times d\mathbf{s}_1}{|\mathbf{s}_1 - \mathbf{r}|^3}, \tag{4}$$

where κ is the quantum of circulation. The filament is represented by the parametric form $\mathbf{s} = \mathbf{s}(\xi, t)$ with the one-dimensional coordinate ξ along the filament. The vector $\mathbf{s}_1$ refers to a point on the filament, and the integration is taken along the filament. Helmholtz's theorem for a perfect fluid states that the vortex moves with the superfluid velocity. Calculating the velocity $\mathbf{v}_s$ at a point $\mathbf{r} = \mathbf{s}$ on the filament causes the integral to diverge as $\mathbf{s}_1 \to \mathbf{s}$. To avoid this divergence, we separate the velocity $\dot{\mathbf{s}}$ of the filament at the point $\mathbf{s}$ into two components [12]:

$$\dot{\mathbf{s}} = \frac{\kappa}{4\pi}\mathbf{s}' \times \mathbf{s}'' \ln\left(\frac{2(\ell_+\ell_-)^{1/2}}{e^{1/4}a_0}\right) + \frac{\kappa}{4\pi}\int_{\mathcal{L}}' \frac{(\mathbf{s}_1 - \mathbf{r}) \times d\mathbf{s}_1}{|\mathbf{s}_1 - \mathbf{r}|^3}. \tag{5}$$

The first term is the localized induction field arising from a curved line element acting on itself, and ℓ_+ and ℓ_- are the lengths of the two adjacent line elements after discretization, separated by the point $\mathbf{s}$. The prime denotes differentiation with respect to the arc length ξ. The mutually perpendicular vectors $\mathbf{s}'$, $\mathbf{s}''$, and $\mathbf{s}' \times \mathbf{s}''$ point along the tangent, the principal normal, and the binormal, respectively, at the point $\mathbf{s}$, and their respective magnitudes are 1, R^{-1}, and R^{-1}, with the local radius R of curvature. The parameter a_0 is the cutoff corresponding to the core radius. Thus, the first term represents the tendency to move the local point $\mathbf{s}$ along the binormal direction with a velocity inversely proportional to R. The

second term represents the non-local field obtained by integrating the integral of Eq. (4) along the rest of the filament, except in the neighborhood of **s**.

Neglecting the non-local terms and replacing Eq. (5) by $\dot{\mathbf{s}} = \beta\, \mathbf{s}' \times \mathbf{s}''$ is referred to as the localized induction approximation (LIA). Here, the coefficient β is defined by $\beta = (\kappa/4\pi) \ln (c \langle R \rangle / a_0)$, where c is a constant of order 1 and $(\ell_+ \ell_-)^{1/2}$ is replaced by the mean radius of curvature $\langle R \rangle$ along the length of the filament. This approximation is believed to be effective for analyzing isotropic dense tangles due to cancellations between non-local contributions.

A better understanding of vortices in a real system is obtained when boundaries are included in the analysis. For this purpose, a boundary-induced velocity field $\mathbf{v}_{s,b}$ is added to $\mathbf{v}_s$, so that the superflow can satisfy the boundary condition of an inviscid flow, that is, that the normal component of the velocity should disappear at the boundaries. To allow for another, presently unspecified, applied field, we include $\mathbf{v}_{s,a}$. Hence, the total velocity $\dot{\mathbf{s}}_0$ of the vortex filament without dissipation is

$$\dot{\mathbf{s}}_0 = \frac{\kappa}{4\pi} \mathbf{s}' \times \mathbf{s}'' \ln \left(\frac{2\,(\ell_+ \ell_-)^{1/2}}{e^{1/4} a_0} \right) + \frac{\kappa}{4\pi} \int_{\mathcal{L}}' \frac{(\mathbf{s}_1 - \mathbf{r}) \times d\mathbf{s}_1}{|\mathbf{s}_1 - \mathbf{r}|^3} + \mathbf{v}_{s,b}(\mathbf{s}) + \mathbf{v}_{s,a}(\mathbf{s}). \tag{6}$$

At finite temperatures, it is necessary to take into account the mutual friction between the vortex core and the normal flow $\mathbf{v}_n$. Including this term, the velocity of **s** is given by

$$\dot{\mathbf{s}} = \dot{\mathbf{s}}_0 + \alpha \mathbf{s}' \times (\mathbf{v}_n - \dot{\mathbf{s}}_0) - \alpha'\, \mathbf{s}' \times [\mathbf{s}' \times (\mathbf{v}_n - \dot{\mathbf{s}}_0)], \tag{7}$$

where α and α' are temperature-dependent friction coefficients [12], and $\dot{\mathbf{s}}_0$ is calculated from Eq. (6).

The numerical simulation method based on this model is described in detail elsewhere [12, 13, 27]. A vortex filament is represented by a single string of points separated by a distance $\Delta\zeta$. The vortex configuration at a given time determines the velocity field in the fluid, thus moving the vortex filaments according to Eqs. (6) and (7). Vortex reconnection should be properly included when simulating vortex dynamics. A numerical study of a classical fluid shows that the close interaction of two vortices leads to their reconnection, chiefly because of the viscous diffusion of the vorticity. Schwarz assumed that two vortex filaments reconnect when they come within a critical distance of one another and showed that statistical quantities such as vortex line density were not sensitive to how the reconnections occur [12, 13]. Even after Schwarz's study, it remained unclear as to whether quantized vortices can actually reconnect. However, Koplik and Levine solved directly the GP equation to show that two closely quantized vortices reconnect even in an inviscid superfluid [28]. More recent simulations have shown that reconnections are accompanied by emissions of sound waves having wavelengths on the order of the healing length [29, 30].

Starting with several remnant vortices under thermal counterflow, Schwarz studied numerically how these vortices developed into a statistical steady vortex tangle [13]. The tangle was self-sustained by the competition between the excitation due to the applied flow and the dissipation through the mutual friction. The numerical results were quantitatively consistent with typical experimental results. This was a significant accomplishment for numerical research.

Here, we shall introduce some quantities that are characteristic of a vortex tangle. The line length density L is defined as the total length of vortex cores in a unit volume. The mean spacing ℓ between vortices is given by $\ell = L^{-1/2}$.

4.2 The Gross-Pitaevskii (GP) Model

In a weakly interacting Bose system, the macroscopic wave function $\Psi(\mathbf{x}, t)$ appears as the order parameter of Bose-Einstein condensation, obeying the Gross-Pitaevskii (GP) equation [2]:

$$i\hbar \frac{\partial \Psi(\mathbf{x},t)}{\partial t} = \left(-\frac{\hbar^2}{2m} \nabla^2 + g|\Psi(\mathbf{x},t)|^2 - \mu \right) \Psi(\mathbf{x},t). \tag{8}$$

Here, $g = 4\pi\hbar^2 m/a$ represents the strength of the interaction characterized by the s-wave scattering length a, m is the mass of each particle, and μ is the chemical potential. Writing $\Psi = |\Psi| \exp(i\theta)$, the squared amplitude $|\Psi|^2$ is the condensate density and the gradient of the phase θ gives the superfluid velocity $\mathbf{v}_s = (\hbar/m)\nabla\theta$, which is a frictionless flow of the condensate. This relation causes quantized vortices to appear with quantized circulation. The only characteristic scale of the GP model is the coherence length defined by $\xi = \hbar / \left(\sqrt{2mg}\, |\Psi| \right)$, which gives the vortex core size. The GP model can explain not only the vortex

dynamics but also phenomena related to vortex cores, such as reconnection and nucleation. However, the GP equation is not applicable quantitatively to superfluid ^{4}He, which is not a weakly interacting Bose system. It is, however, applicable to Bose-Einstein condensation of a dilute atomic Bose gas [2].

5. QUANTIZED VORTICES IN A ROTATING BEC

This section describes the typical phenomenon of quantum hydrodynamics of atomic BECs, namely the vortex lattice formation in a rotating BEC. What happens if we rotate a cylindrical vessel with a classical viscous fluid inside? Even if the fluid is initially at rest, it starts to rotate and eventually reaches a steady rotation with the same rotational speed as the vessel. In that case, one can say that the system contains a vortex that mimics solid-body rotation.[3] A rotation of arbitrary angular velocity can be sustained by a single vortex. However, this does not occur in a quantum fluid. Because of quantization of circulation, superfluids respond to rotation, not with a single vortex, but with a lattice of quantized vortices. Feynman noted that in uniform rotation with angular velocity Ω the rot of the superfluid velocity is the circulation per unit area, and since the rot is 2Ω, a lattice of quantized vortices with number density $n_0 = \mathrm{rot}\upsilon_s/\kappa = 2\Omega/\kappa$ ("Feynman's rule") arranges itself parallel to the rotation axis [4]. Such experiments were performed for superfluid ^{4}He: Packard *et al*. visualized vortex lattices on the rotational axis by trapping electrons along the cores [31, 32].

This idea has also been applied to atomic BECs. Several groups have observed vortex lattices in rotating BECs [23, 24, 25, 33]. Among them, Madison *et al*. directly observed nonlinear processes such as vortex nucleation and lattice formation in a rotating ^{87}Rb BEC [25]. By sudden application of a rotation along the trapping potential, an initially axisymmetric condensate undergoes a collective quadrupole oscillation to an elliptically deformed condensate. This oscillation continues for a few hundred milliseconds with gradually decreasing amplitude. Then the axial symmetry of the condensate is recovered and vortices enter the condensate through its surface, eventually settling into a lattice configuration.

This observation has been reproduced by a simulation of the Gross-Pitaevskii (GP) equation for the macroscopic wavefunction $\Psi(\mathbf{x}, t) = |\Psi(\mathbf{x}, t)|e^{i\theta(\mathbf{x}, t)}$ in two-dimensional [34, 35] and three-dimensional [36] spaces. The corresponding GP equation in a frame rotating with frequency $\Omega = \Omega\hat{\mathbf{z}}$ is given by

$$(i-\gamma)\,\hbar\frac{\partial\Psi(\mathbf{x}, t)}{\partial t} = \left[-\frac{\hbar^2}{2m}\nabla^2 + V_{\mathrm{ex}}(\mathbf{x}) + g|\Psi(\mathbf{x}, t)|^2 - \Omega L_z\right]\Psi(\mathbf{x}, t). \tag{9}$$

Here V_{ex} is a trapping potential, and $L_z = -i\hbar(x\partial_y - y\partial_x)$ is the angular momentum along the rotational axis. The interparticle potential V_{int} is approximated by a short-range interaction $V_{\mathrm{int}} \simeq g\delta(\mathbf{x} - \mathbf{x}')$, where $g = 4\pi\hbar^2 a/m$ is a coupling constant characterized by the s-wave scattering length a. The term γ indicates phenomenological dissipation.[4]

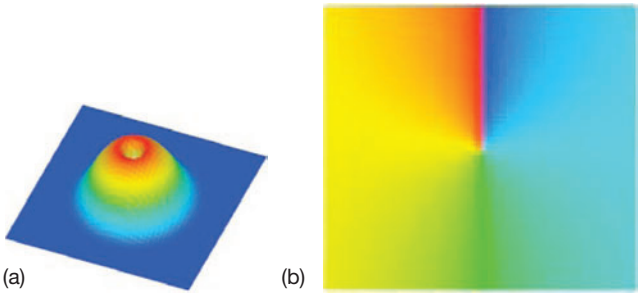

Fig. 2. Profile of (a) the condensate density and (b) the phase of the macroscopic wavefunction when there is a quantized vortex in a trapped BEC [21]. The value of the phase varies continuously from 0 (red) to 2π (blue).

[3]Thin boundary layers of the Ekman and Stewartson types can appear in a rotating classical fluid, but we do not consider such complicated structures here.

[4]We used $\gamma = 0.03$ in this simulation [34, 35]. The vortex state corresponds to the minimum of the free energy in a rotating frame. In order to take the system from some high-energy vortex-free state to the minimum, we need some dissipation. The calculation without dissipation never forms the vortex lattice. The value of γ is tuned so that the GP equation can explain some experiments observing the damping of the collective mode.

Figure 2 shows the profile of the condensate density $|\Psi(\mathbf{x}, t)|^2$ and the phase $\theta(\mathbf{x}, t)$ when there is a quantized vortex in a trapped BEC. The density has a hole representing the vortex core. The phase has a branch cut between 0 and 2π, and the edge of the branch cut corresponds to the vortex core around which the phase rotates by 2π as the superflow circulates. One can therefore clearly identify the vortex both in the density and the phase.

A typical two-dimensional numerical simulation of Eq. (9) [34, 35] for the vortex lattice formation is shown in Fig. 3, where the condensate density and the phase are displayed together. The trapping potential is

$$V_{\rm ex} = \frac{1}{2} m\omega^2 \left[(1 + \epsilon_x) x^2 + (1 + \epsilon_y)\, y^2 \right], \tag{10}$$

where $\omega = 2\pi \times 219$ Hz, and the parameters $\epsilon_x = 0.03$ and $\epsilon_y = 0.09$ describe small deviations from axisymmetry corresponding to experiments [24, 25]. We first prepare an equilibrium condensate trapped in a stationary potential; the size of the condensate cloud is determined by the Thomas-Fermi radius $R_{\rm TF}$. When we apply a rotation with $\Omega = 0.7\omega$, the condensate becomes elliptic and performs a quadrupole oscillation [Fig. 3(a)]. Then, the boundary surface of the condensate becomes unstable and generates ripples that propagate along the surface [Fig. 3(b)]. As stated previously, it is possible to identify quantized vortices in the phase profile also. As soon as the rotation starts, many vortices appear in the low-density region outside of the condensate [Fig. 3(a)]. Since quantized vortices are excitations, their nucleation increases the energy of the system. Because of the low density in the outskirts of the condensate, however, their nucleation contributes little to the energy and angular momentum.[5] Since these vortices outside of the condensate are not observed in the density profile, they are called "ghost vortices". Their movement toward the Thomas-Fermi surface excites ripples [Fig. 3(b)]. It is not easy for these ghost vortices to enter the condensate, because that would increase both the energy and angular momentum. Only some vortices enter the condensate cloud to become "real vortices" wearing the usual density profile of quantized vortices [Fig. 3(d)], eventually forming a vortex lattice [Fig. 3 (e) and (f)]. The number of vortices forming a lattice is given by "Feynman's rule" $n_0 = 2\Omega/\kappa$. The numerical results agree quantitatively with these observations.

Note the essence of the dynamics. The initial state has no vortices in the absence of rotation. The final state is a vortex lattice corresponding to rotational frequency Ω. In order to go from the initial to the final state, the system makes use of as many excitations as possible, such as vortices, quadruple oscillation, and surface waves. We refer the readers to Ref. 35 for details.

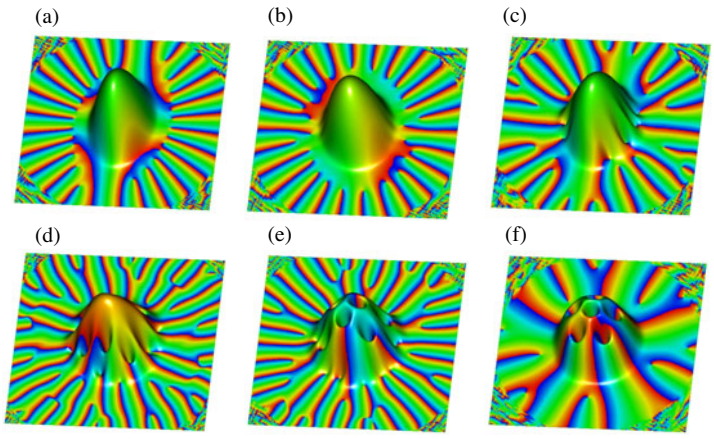

Fig. 3. Dynamics of vortex lattice formation in a rotating BEC [21]. The figure simultaneously shows both the condensate density and phase. They are bird's -eye pictures of the distribution of the condensate density, and the color shows the phase continuously from 0 (red) to 2π (blue). The graphs are at (a) t = 63 ms, (b) 305 ms, (c) 350 ms, (d) 410 ms, (e) 450 ms, and (f) 850 ms after the start of the rotation.

[5]Actually the vortex-antivortex pairs are nucleated in the low-density region. Then the vortices parallel to the rotation are dragged into the Thomas-Fermi surface, while the antivortices are repelled to the outskirts.

6. MODERN RESEARCH TRENDS OF QUANTUM TURBULENCE IN SUPERFLUID HELIUM

Most older experimental studies on QT were devoted to thermal counterflow. Since this flow has no classical analogue, these studies do not contribute greatly to the understanding of the relationship between CT and QT. Since the mid 1990s, important experimental studies on QT that did not focus on thermal counterflow have been published.

6.1 New Experiments on Energy Spectra

The first important contribution was made by Maurer and Tabeling [37], who confirmed experimentally the Kolmogorov spectrum in superfluid ^{4}He for the first time. A turbulent flow was produced in a cylinder by driving two counter-rotating disks. The authors observed the local pressure fluctuations to obtain the energy spectrum. The experiments were conducted at three different temperatures 2.3 K, 2.08 K, and 1.4 K. Both above and below the λ point, the Kolmogorov spectrum was confirmed. The observed behavior above the λ point is not surprising because the system is a classical viscous fluid. However, it is not trivial to understand the Kolmogorov spectrum at two different temperatures below the λ point.

The next significant step was a series of experiments on grid turbulence performed for superfluid ^{4}He above 1 K by the Oregon group [38, 39, 40, 41]. The flow through a grid is usually used to generate turbulence in classical fluid dynamics [14]. At a sufficient distance behind the grid, the flow displays a form of homogeneous isotropic turbulence. This method has also been applied to superfluid helium. In the experiments by the Oregon group, the helium was contained in a channel with a square cross section, through which a grid was pulled at a constant velocity. A pair of second-sound transducers was set into the walls of the channel. When a vortex tangle appeared in a channel, it was detected by second-sound attenuation [17]. The decay of the vorticity of the tangle created behind the towed grid was observed by the pair of transducers. In combining the observations with the decay of the turbulence, the authors made some assumptions. In fully developed turbulence, the energy dissipation rate can be shown to be given as $\epsilon = \nu\langle\omega^2\rangle$, where $\langle\omega^2\rangle$ is the mean square vorticity (rot $\mathbf{v}$) in the flow [42]. The authors assumed that a similar formula applies in superfluid helium above 1 K. They noted that the quantity $\kappa^2 L^2$ would be a measure of the mean square vorticity in the superfluid component. Hence, they assumed that in grid turbulence the dissipation rate is given by $\epsilon = \nu'\kappa^2 L^2$ with an effective kinematic viscosity ν'. In order to combine this representation with the observations of second-sound attenuation for grid turbulence, the authors furthermore assumed that a quasi-classical flow appears at length scales much greater than ℓ. The flow is thought to come from a mechanism coupling the superfluid and the normal fluid by mutual friction, causing the fluid to behave like a one-component fluid [43]. By choosing suitable values of ν' as a function of temperature [41], it was found that κL decays as $t^{-3/2}$.

This characteristic decay $L \propto t^{-3/2}$ is quite important, because it is related to the Kolmogorov spectrum. Thus, we herein present the simple argument given in a previous review article [17]. We assume that a turbulent fluid obeys the Kolmogorov spectrum of Eq. (3) in the inertial range of $D^{-1} < k < k_d$ with $D^{-1} << k_d$. The total energy is approximately given by

$$E = \int_{D^{-1}}^{k_d} C\varepsilon^{2/3} k^{-5/3}\, dk \approx \frac{3}{2} C\varepsilon^{2/3} D^{2/3}. \tag{11}$$

If the turbulence decays slowly with time and the dissipation rate ε is assumed to be time-dependent, we can write

$$\varepsilon = -\frac{dE}{dt} = -C\varepsilon^{-1/3} D^{2/3}\, \frac{d\varepsilon}{dt}. \tag{12}$$

The solution gives the time-dependence of ε:

$$\varepsilon = 27\ C^3 \mathrm{D}^2 (t + t_0)^{-3}, \tag{13}$$

where t_0 is a constant. Combining Eq. (13) with the above formula of ε gives the decay of L:

$$L = \frac{(3C)^{3/2} D}{\kappa \nu'^{1/2}} (t + t_0)^{-3/2}. \tag{14}$$

This behavior has been observed, and a quantitative comparison with observations at any temperature gives ν' as a function of temperature. The observation of the decay $L \sim t^{-3/2}$ indicates that the Kolmogorov spectrum applies in turbulence, although it is not necessarily direct proof. Note that this simple analysis is applicable only when the maximum length scale of the turbulent energy saturates at the size of the channel. For the complete dynamics, a more complicated decay of vortices has been observed and has been found to be consistent with the classical model of the Kolmogorov spectrum [38, 39, 40]. This type of decay is also observed at very low temperatures in the turbulence induced by an impulsive spin down for superfluid ^{4}He [44] and in grid turbulence for the B phase of superfluid ^{3}He [45, 46][6].

6.2 Energy Spectra at Finite Temperatures

These observations lead us to inquire as to the nature of the velocity field that gives rise to the observed energy spectrum. Vinen considered the situation theoretically [43] and proposed that it is likely that the superfluid and normal fluid are coupled by mutual friction at scales larger than the characteristic scale ℓ of the vortex tangle. If so, the two fluids behave as a one-component fluid at these scales, where mutual friction does not cause dissipation. Since the normal fluid is viscous, the two coupled fluids can be turbulent and obey the Kolmogorov spectrum. The observation of the energy spectrum by Maurer *et al.* and Stalp *et al.* should support the idea of the coupled dynamics of two fluids. At small scales, the two fluids should be decoupled, so that both mutual friction and normal fluid viscosity operate. What then happens to the energy spectrum? Although theoretical consideration has been given to this problem [47], the answer remains controversial and has not yet been clarified. While this is an important problem, it is not investigated in the present article.

6.3 Modern Research Trends

The following three trends are currently the primary research areas in QT in superfluid helium. The first is the energy spectra and the dissipation mechanism at zero temperature [48]. The second is QT created by vibrating structures [49]. The third is visualization of QT [50]. The remainder of this section is devoted to the review of these related topics.

6.4 Energy spectra and Dissipation at Zero Temperature

What happens to QT at zero temperature is not so trivial. The first problem is determining the nature of the energy spectrum of turbulence for the pure superfluid component [48]. If QT has a classical analogue, the energy spectrum is expected to obey the Kolmogorov law and have an inertial range in which the energy is transferred self-similarly from large to small scales. In QT at zero temperature, any rotational motion should be carried by quantized vortices. Since quantized vortices are definite topological defects, the cascade can be attributed directly to their dynamics, which is different from the case for CT. In a classical case the Richardson cascade is only schematic. The second problem is determining how the energy is transferred from large to small scales. There is no dissipative mechanism at large scales. However, some dissipative mechanism should operate at small scales, as described below. A vortex tangle has a characteristic scale ℓ, which is defined by the mean spacing between vortex lines. At scales greater than ℓ, a Richardson cascade should transfer the energy through the breakup of vortices. However, the Richardson cascade becomes ineffective at small scales, especially below ℓ. What mechanism cascades the energy instead of the Richardson cascade at these scales? The third problem is understanding the dissipation in the system. The first possibility is acoustic emission at vortex reconnections. In classical fluid dynamics, vortex reconnections cause acoustic emission. In quantum fluids, numerical simulations of the GP model show acoustic emission at every reconnection event [29]. However, this mechanism is thought to be unimportant because of the very short coherence length. The second possible mechanism is the radiation of sound (phonons) by the oscillatory motion of vortex cores. We will return to these mechanisms, as well as other possibilities.

[6]A ^{3}He atom is a Fermion, another isotope of helium. Liquid ^{3}He becomes superfluid below about 1mK through the BCS (Bardeen-Cooper - Schrieffer) mechanism which works in usual superconductors. Superfluid ^{3}He is anisotropic, yielding multicomponent order parameters. Depending on pressure and temperature, the A and B phases appear, and another A1 phase is stabilized under a magnetic field.

6.4.1 Energy Spectra

No experimental studies have addressed this issue directly, although a few numerical studies have been conducted. The first study was performed by Nore *et al*. using the GP model [51, 52]. They solved the GP equation numerically starting from Taylor-Green vortices, and followed the time development. The quantized vortices become tangled and the energy spectra of the incompressible kinetic energy seemed to obey the Kolmogorov law for a short period, although the energy spectra eventually deviated from the Kolmogorov law. The second study was performed by the vortex filament model[53], and the third study was performed by the modified GP model [54, 55].

6.4.2 Energy Spectra by the Vortex Filament Model

Using the vortex filament model, Araki *et al*. generated a vortex tangle arising from Taylor-Green vortices and obtained an energy spectrum consistent with the Kolmogorov law[53]. It would be informative to describe how to obtain the energy spectra under the vortex filament model. The energy spectrum is calculated by Fourier transform of the superfluid velocity $\mathbf{v}_s(\mathbf{r})$, which is determined by the configuration of quantized vortices. Thus, the energy spectrum can be calculated directly from the configuration of the vortices. Using the Fourier transform $\mathbf{v}_s(\mathbf{k}) = (2\pi)^{-3} \int d\mathbf{r}\mathbf{v}_s(\mathbf{r}) \exp(-i\mathbf{k}\cdot\mathbf{r})$ and Parseval's theorem $\int d\mathbf{k}|\mathbf{v}_s(\mathrm{k})|^2 = (2\pi)^{-3} \int d\mathbf{r}|\mathbf{v}_s(\mathbf{r})|^2$, the kinetic energy of the superfluid velocity per unit mass is

$$E = \frac{1}{2}\int d\mathbf{r}|\mathbf{v}_s(\mathbf{r})|^2 = \frac{(2\pi)^3}{2}\int d\mathbf{k}|\mathbf{v}_s(\mathbf{k})|^2. \tag{15}$$

The vorticity $\omega(\mathbf{r}) = \mathrm{rot}\mathbf{v}_s(\mathbf{r})$ is represented in Fourier space as $\mathbf{v}_s(\mathbf{k}) = i\mathbf{k} \times \omega(\mathbf{k})/|\mathbf{k}|^2$, so that we have $E = ((2\pi)^3/2) \int d\mathbf{k}|\omega(\mathbf{k})|^2/|\mathbf{k}|^2$. The vorticity is concentrated on the vortex filament, represented by

$$\omega(\mathbf{r}) = \kappa \int \mathrm{d}\xi\ \mathbf{s}'(\xi)\ \delta(\mathrm{s}(\xi) - \mathbf{r}), \tag{16}$$

which can be rewritten as

$$\omega(\mathbf{k}) = \frac{\kappa}{(2\pi)^2}\int d\xi\ \mathbf{s}'(\xi) \exp(-i\mathbf{s}(\xi)\ \cdot\ \mathbf{k}). \tag{17}$$

Using the definition of the energy spectrum $E(k)$ from $E = \int_0^\infty dkE(k)$, these relations yield

$$E(k) = \frac{\kappa^2}{2(2\pi)^3}\int \frac{d\Omega_k}{|\mathbf{k}|^2}\int\int d\xi_1\ d\xi_2\ \mathbf{s}'(\xi_1)\cdot\mathbf{s}'(\xi_2) \exp(-i\mathbf{k}\ \cdot\ (\mathbf{s}(\xi_1) - \mathbf{s}(\xi_2))), \tag{18}$$

where $d\Omega_k = k^2 \sin\theta_k d\theta_k d\phi_k$ is the volume element in spherical coordinates.

Starting from a Taylor-Green vortex and following the vortex motion under the full Biot-Savart law without mutual friction, Araki *et al*. obtained a roughly homogeneous and isotropic vortex tangle [53]. This was a decaying turbulence, dissipated by the cutoff of the smallest vortices, the size of which is comparable to the numerical space resolution. Initially, the energy spectrum has a large peak at the largest scale, where the energy is concentrated. The spectrum changes as the vortices become homogeneous and isotropic. The energy spectrum of the vortex tangle at some late stage was quantitatively consistent with the Kolmogorov spectrum in thesmall k region. By monitoring the development of the vortex size distribution, the decay of a tangle is found to be sustained by a Richardson cascade process. These results support the quasi-classical picture of the inertial range in QT at very low temperatures.

6.4.3 Energy Spectra by the GP Model

As the third trial, the Kolmogorov spectra were confirmed for both decaying [54] and steady [55] QT by the modified GP model. The normalized GP equation is

$$i\frac{\partial}{\partial t}\Phi(\mathbf{x}, t) = [-\nabla^2 - \mu + g|\Phi(\mathbf{x}, t)|^2]\ \Phi(\mathbf{x}, t), \tag{19}$$

which determines the dynamics of the macroscopic wave function $\Phi(\mathbf{x}, t) = f(\mathbf{x}, t) \exp[i\phi(\mathbf{x}, t)]$. The condensate density is $|\Phi(\mathbf{x}, t)|^2 = f(\mathbf{x}, t)^2$, and the superfluid velocity $\mathbf{v}(\mathbf{x}, t)$ is given by $\mathbf{v}(\mathbf{x}, t) = 2\nabla\phi(\mathbf{x}, t)$. The vorticity $\omega(\mathbf{x}, t) = \mathrm{rot}\mathbf{v}(\mathbf{x}, t)$ vanishes everywhere in a single-connected region of the fluid and thus all rotational flow is carried by quantized vortices. In the core of each vortex, $\Phi(\mathbf{x}, t)$ vanishes so that the circulation around the core is quantized by 4π. The vortex core size is given by the healing length $\xi = 1/f\sqrt{g}$.

Note that the hydrodynamics described by the GP model is compressible, which is different from the incompressible case of the vortex filament model. The total number of condensate particles is $N = \int d\mathbf{x}|\Phi(\mathbf{x}, t)|^2$ and the total energy is

$$E(t) = \frac{1}{N}\int d\mathbf{x}\, \Phi^*(\mathbf{x}, t)\left[-\nabla^2 + \frac{g}{2} f(\mathbf{x}, t)^2\right]\Phi(\mathbf{x}, t), \tag{20}$$

which is represented by the sum of the interaction energy $E_{int}(t)$, the quantum energy $E_q(t)$, and the kinetic energy $E_{kin}(t)$ [51, 52]:

$$E_{int}(t) = \frac{g}{2N}\int d\mathbf{x}\, f(\mathbf{x}, t)^4,\ E_q(t) = \frac{1}{N}\int d\mathbf{x}\, [\nabla f(\mathbf{x}, t)]^2,$$
$$E_{kin}(t) = \frac{1}{N}\int d\mathbf{x}\, [f(\mathbf{x}, t)\nabla\phi(\mathbf{x}, t)]^2. \tag{21}$$

The kinetic energy is furthermore divided into a compressible part $E^c_{kin}(t)$ due to compressible excitations and an incompressible part $E^i_{kin}(t)$ due to vortices. If the Kolmogorov spectrum is observed, the spectrum should be that for the incompressible kinetic energy $E^i_{kin}(t)$.

The failure to obtain the Kolmogorov law under the pure GP model [51, 52] would be attributable to the following reasons. Note that the situation here is decaying turbulence. Although the total energy $E(t)$ was conserved, $E^i_{kin}(t)$ decreased with increasing $E^c_{kin}(t)$. This was because many compressible excitations were created through repeated vortex reconnections [29, 30] and disturbed the Richardson cascade of quantized vortices even at large scales.

Kobayashi and Tsubota overcame the difficulties of Nore *et al*. and obtained the Kolmogorov spectra in QT and clearly revealed the energy cascade [54, 55]. They performed numerical calculation for the Fourier transformed GP equation with dissipation:

$$(i - \tilde{\gamma}(\mathbf{k}))\frac{\partial}{\partial t}\tilde{\Phi}(\mathbf{k}, t) = [k^2 - \mu(t)]\,\tilde{\Phi}(\mathbf{k}, t)$$
$$+ \frac{g}{V^2}\sum_{\mathbf{k}_1, \mathbf{k}_2}\tilde{\Phi}(\mathbf{k}_1, t)\,\tilde{\Phi}^*(\mathbf{k}_2, t)\,\tilde{\Phi}(\mathbf{k} - \mathbf{k}_1 + \mathbf{k}_2, t). \tag{22}$$

Here, $\tilde{\Phi}(\mathbf{k}, t)$ is the spatial Fourier component of $\Phi(\mathbf{x}, t)$ and V is the system volume. The healing length is given by $\xi = 1/|\Phi|\sqrt{g}$. The dissipation should have the form $\tilde{\gamma}(\mathbf{k}) = \gamma_0\,\theta(k - 2\pi/\xi)$ with the step function θ, which dissipates only the excitations smaller than ξ. This form of dissipation can be justified by the coupled analysis of the GP equation for the macroscopic wave function and the Bogoliubov-de Gennes equations for thermal excitations [56].

First, Kobayashi *et al*. confirmed the Kolmogorov spectra for decaying turbulence [54]. To obtain a turbulent state, they started the calculation from an initial configuration in which the density was uniform and the phase of the wave function had a random spatial distribution. The initial wave function was dynamically unstable and soon developed into fully developed turbulence with many quantized vortex loops. The spectrum $E^i_{kin}(k,t)$ of the incompressible kinetic energy was then found to obey the Kolmogorov law.

A more elaborate analysis of steady QT was performed by introducing energy injection at large scales as well as energy dissipation at small scales [55]. Energy injection at large scales was effected by moving a random potential $V(\mathbf{x}, t)$. Numerically, Kobayashi *et al*. placed random numbers between 0 and V_0 in space-time $(\mathbf{x}, t)$ at intervals of X_0 for space and T_0 for time and connected them smoothly using a four-dimensional spline interpolation. The moving random potential exhibited a Gaussian two-point correlation:

$$\langle V(\mathbf{x}, t)\, V(\mathbf{x}', t')\rangle = V_0^2 \exp\left[-\frac{(\mathbf{x}-\mathbf{x}')^2}{2X_0^2} - \frac{(t-t')^2}{2T_0^2}\right]. \tag{23}$$

This moving random potential had a characteristic spatial scale of X_0. Small vortex loops were first nucleated by the random potential, growing to the scale of X_0 by its motion subjected to Eq. (23). The vortex loops were then cast into the Richardson cascade. If steady QT is obtained by the balance between the energy injection and the dissipation, it should have an energy-containing range of $k < 2\pi/X_0$, an inertial range of $2\pi/X_0 < k < 2\pi/\xi$, and an energy-dissipative range of $2\pi/\xi < k$.

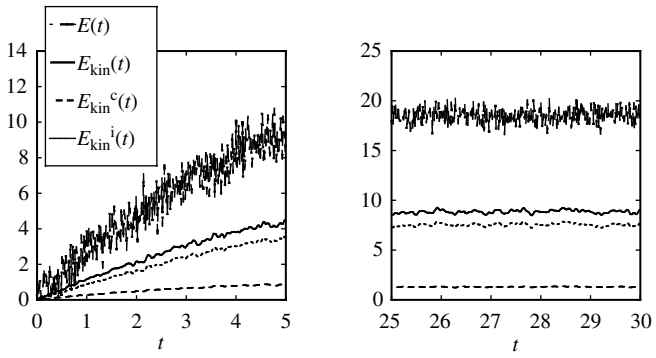

Fig. 4. Results of numerical simulation of the GP equation with energy injection at large scales and energy dissipation at small scales. Time development of the total energy $E(t)$, the kinetic energy $E_{kin}(t)$, the compressible kinetic energy $E^c_{kin}(t)$, and the incompressible kinetic energy $E^i_{kin}(t)$ at (a) the initial stage $0 \le t \le 5$ and (b) a later stage $25 \le t \le 30$ [55]. The system is found to be statistically steady at the later stage.

A typical simulation of steady turbulence was performed for $V_0 = 50$, $X_0 = 4$, and $T_0 = 6.4 \times 10^{-2}$. The dynamics started from the uniform wave function. Figure 4 shows the time development of each energy component. The moving random potential nucleates sound waves as well as vortices, but both figures show that the incompressible kinetic energy $E^i_{kin}(t)$ due to vortices is dominant in the total kinetic energy $E_{kin}(t)$. The four energies are almost constant for $t \lesssim 25$, and steady QT was obtained.

Such a steady QT enables us to investigate the energy cascade. Here, we expect an energy flow in wavenumber space similar to that in Fig. 5. The upper half of the diagram shows the kinetic energy $E^i_{kin}(t)$ of quantized vortices, and the lower half shows the kinetic energy $E^c_{kin}(t)$ of compressible excitations. In the energy-containing range $k < 2\pi/X_0$, the system receives incompressible kinetic energy from the moving random potential. During the Richardson cascade process of quantized vortices, the energy flows from small to large k in the inertial range $2\pi/X_0 < k < 2\pi/\xi$. In the energy-dissipative range $2\pi/\xi < k$, the incompressible kinetic energy transforms to compressible kinetic energy through reconnections of vortices or the disappearance of small vortex loops. The moving random potential also creates long-wavelength compressible sound waves, which are another source of compressible kinetic energy and also produce an interaction with vortices. However, the effect of sound waves is weak because $E^i_{kin}(t)$ is much larger than $E^c_{kin}(t)$, as shown in Fig. 4.

This cascade can be confirmed quantitatively by checking whether the energy dissipation rate ε of $E^i_{kin}(t)$ is comparable to the flux of energy $\Pi(k, t)$ through the Richardson cascade in the inertial range. Although the details are described in Reference 55, $\Pi(k, t)$ is found to be approximately independent of k and comparable to ε. As shown in Fig. 6 (b), the energy spectrum is quantitatively consistent with the Kolmogorov law in the inertial range $2\pi/X_0 < k < 2\pi/\xi$, which is equivalent to $0.79 \lesssim k \lesssim 6.3$. It is interesting to focus on Richardson cascade. Richardson cascade is only conceptual in CT, while it is genuine in QT in which vortices are identified definitely. Actually we observe lots of events of the splitting of a vortex into smaller vortices in the turbulence state. The situation is more difficult to understand in CT. This is one of the reasons why we believe that QT is simper than CT.

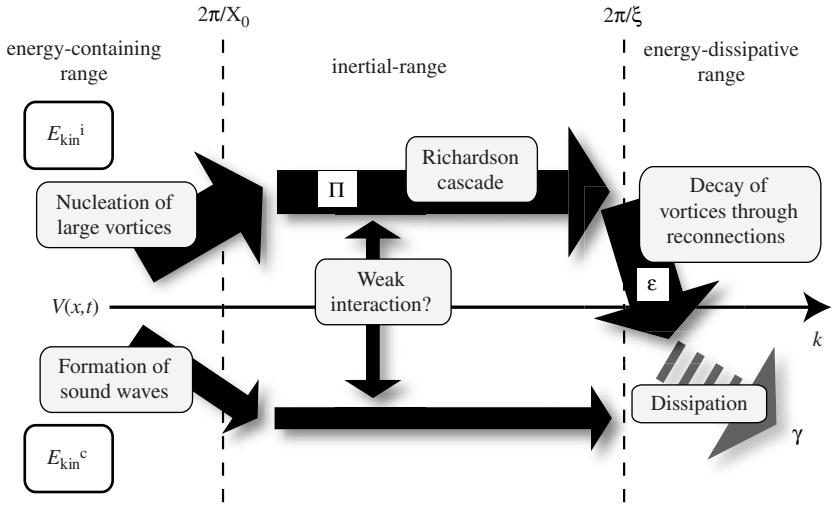

Fig. 5. Schematic diagram of the flow of the incompressible kinetic energy $E^i_{kin}(t)$ (upper half of diagram) and compressible kinetic energy $E^c_{kin}(t)$ (lower half) in wavenumber space in the steady turbulence by the GP equation[55]. The energy is injected in the energy-containing range ($k < 2\pi/X_0$) through the moving random potential $V(\mathbf{x},t)$, leading to nucleation of vortices in E^i_{kin} and formation of sound waves E^c_{kin}. In E^i_{kin} the energy is trasferred in the inertial-range ($2\pi/X_0 < k < 2\pi/\xi$) through the Richardson cascade of quantized vortices with the energy flux Π, then dissipated with the rate ϵ in the energy-dissipative range ($2\pi/\xi < k$) by the dissipative term of γ. There may be some energy cascade in E^c_{kin} too and some weak interaction with E^i_{kin}, which is not clear currently.

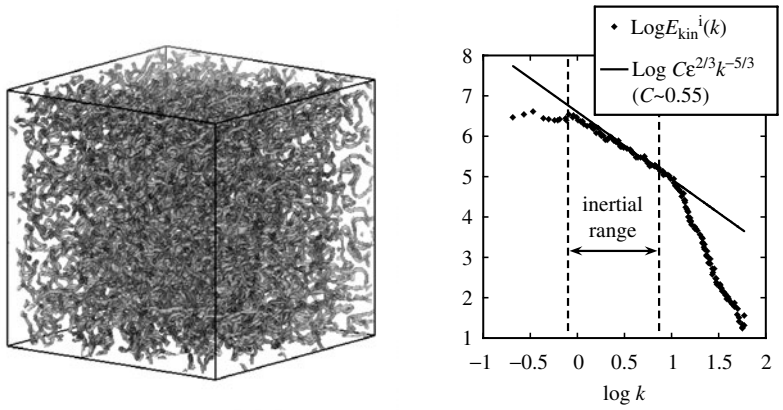

Fig. 6. A steady quantum turbulence obtained numerically by the GP equation. (a) A typical vortex tangle. (b) Energy spectrum $E^i_{kin}(k,t)$ for QT. The plotted points are from an ensemble average of 50 randomly selected states at $t > 25$. The solid line is the Kolmogorov law [55]. The inertial range corresponds to $2\pi/X_0 < k < 2\pi/\xi$ (see Fig.5), in which the spectrum obeys the Kolmogorov law. The Kolmogorov constant $C \sim 0.55$ is lower than the usual value $C \sim 1.4$, the reason of which is not known.

Kobayashi *et al*. studied the decay of QT under the same formulation [57]. After obtaining a steady tangle, they switched off the motion of the random potential and found that L decayed as $t^{-3/2}$.

6.4.4 The Kelvin-wave Cascade

The arguments in the last section were chiefly limited to the large scale, usually larger than the mean spacing ℓ of a vortex tangle, in which the Richardson cascade is effective for transferring the energy from large to small scales. Here, we should consider what happens at smaller scales, for which the

Richardson cascade should be less effective. The most probable scenario is the Kelvin-wave cascade. A Kelvin-wave is a deformation of a vortex line into a helix with the deformation propagating as a wave along the vortex line [58]. Kelvin-waves were first observed by making torsional oscillations in uniformly rotating superfluid ^{4}He [59, 60]. The approximate dispersion relation for a rectilinear vortex is $\omega_k = (\kappa k^2)/(4\pi)(\ln(1/ka_0)+c)$ with a constant $c \sim 1$. Note that this k is the wavenumber of an excited Kelvin-wave and is different from the wavenumber used for the energy spectrum in the last subsection. At a finite temperature, a significant fraction of normal fluid damps Kelvin-waves through mutual friction. At very low temperatures, however, mutual friction does not occur, and the only possible mechanism of dissipation is the radiation of phonons [61]. Phonon radiation becomes effective only when the frequency becomes very high, typically on the order of GHz ($k \sim 10^{-1}$ nm^{-1}), so a mechanism is required to transfer the energy to such high wavenumbers in order for Kelvin-waves to be damped. An early numerical simulation based on the vortex filament model showed that Kelvin-waves are unstable to the buildup of side bands [62]. This indicates the possibility that nonlinear interactions between different Kelvin-wave numbers can transfer energy from small to large wavenumbers, namely the Kelvin-wave cascade. This idea was first suggested by Svistunov [63] and was later developed and confirmed through theoretical and numerical analyses by Kivotides *et al*. [64], Vinen *et al*. [65], and Kozik and Svistunov [66, 67, 68].

6.4.5 Classical-quantum Crossover

An important trend is investigation of the nature of the transition between the Richardson and the Kelvin-wave cascades. Turbulence at scales larger than the mean vortex spacing obeys the Kolmogorov law with a Richardson cascade. In this regime, the nature of individual vortices is not relevant, and the large-scale velocity field created collectively by the vortices mimics classical turbulent behavior. This regime may therefore be called classical. In contrast, at length scales smaller than the mean vortex spacing the energy is transferred along each vortex through a Kelvin-wave cascade; this regime has no classical analog and can be called quantum. Several theoretical considerations of the classical-quantum crossover have been proposed.

L'vov *et al*. theoretically discussed a bottleneck crossover between the two regions [69]. Their investigation was based on the idea that a vortex tangle obeying the Kolmogorov spectrum is polarized to some degree, and they viewed the vortex tangle as a set of vortex bundles. When they tried to connect the energy spectra between two cascades, a serious mismatch occurred at the crossover scale between the classical and quantum spectra. This mismatch prevented the energy flux from propagating fully through the crossover region, which is referred to as the bottleneck effect. In order to remedy this mismatch, L'vov *et al*. used warm cascade solutions [72] and proposed a thermal-equilibrium type spectrum between the classical and quantum spectra. The analysis of L'vov *et al*. was based on the assumption that the coarse-grained macroscopic picture of quantized vortices remains valid down to a scale of ℓ. Without this assumption, Kozik and Svistunov theoretically investigated the details of the structure of the vortex bundle in the crossover region [70, 71]. Depending on the types of vortex reconnections, the crossover range near ℓ was further divided into three subranges, resolving the mismatch between two cascades. However, this topic is not yet fixed, and remains controversial.

6.4.6 Possible Dissipation Mechanism at Zero Temperature

Here, we should investigate the possible dissipation mechanisms of QT at very low temperatures, in which the normal fluid component is so negligible that mutual friction does not occur. In this case, there is no dissipation at relatively large scales, and dissipation can only occur at small scales. Energy at large scales should be transferred to smaller scales by a Richardson cascade and then a Kelvin-wave cascade until the dissipation becomes effective. The description presented herein is only schematic. Please refer to other papers for a more detailed discussion [43, 17].

Dissipation of QT at zero temperature was first proposed by Feynman [4]. Feynman suggested that a large vortex loop should be broken up into smaller loops through repeated vortex reconnections, which is essentially identical to the Richardson cascade. Feynman thought that the smallest vortex ring having a radius comparable to the atomic scale must be a roton, although this belief is not currently accepted universally. Later, Vinen considered the decay of superfluid turbulence in order to understand his experimental results for thermal counterflow [7, 8], leading him to propose Vinen's equation [9]. Although the experiments were performed at finite temperatures, the physics is important in order to study the decay of QT, as described briefly herein. Vortices in turbulence are assumed to be

approximately evenly spaced with a mean spacing of $\ell = L^{-1/2}$. The energy of the vortices then spreads from the vortices of wavenumber $1/\ell$ to a wide range of wavenumbers. The overall decay of the energy is governed by the characteristic velocity $v_s = k/2\,\pi\ell$ and the time constant ℓ/v_s of the vortices of size ℓ, giving

$$\frac{dv_s^2}{dt} = -\chi \frac{v_s^2}{\ell/v_s} = \chi \frac{v_s^3}{\ell}, \tag{24}$$

where χ is a dimensionless parameter that is generally dependent on temperature. Rewriting this equation using L, we obtain

$$\frac{dL}{dt} = -\chi \frac{\kappa}{2\pi} L^2. \tag{25}$$

This is called Vinen's equation. The original Vinen's equation also includes a term of vortex amplification, which is not shown here. This equation describes the decay of L, the solution of which is

$$\frac{1}{L} = \frac{1}{L_0} + \chi \frac{\kappa}{2\pi} t, \tag{26}$$

where L_0 is L at $t = 0$. The thermal counterflow observations are well described by this solution, which gives the values of χ as a function of temperature [9]. The decay at finite temperatures is due to mutual friction. The value of χ at zero temperature is obtained by a numerical simulation of the vortex filament model [27].

What causes the different types of decay of $L \sim t^{-3/2}$ of Eq. (14) and $L \sim t^{-1}$ of Eq. (27)? The different types of decay originate from the different structures of vortex tangles in QT. When the energy spectrum of a vortex tangle obeys the Kolmogorov law, the tangle is self-similar in the inertial range, and most energy is in the largest vortex. The then decays as $L \sim t^{-3/2}$, as described in Section 4.1. If a vortex tangle is random and has little correlation, however, the only length scale is $\ell = L^{-1/2}$, yielding a decay of $L \sim t^{-1}$, as described herein. Therefore, the observation of how L decays is helpful in understanding the structure of vortex tangles in QT. The two kinds of decay are actually observed in superfluid ^{4}He at very low temperatures [73].

However, these studies do not explain what happens to QT at zero temperature at small scales. There are several possibilities. The first is acoustic emission at vortex reconnections. In classical fluid dynamics it is known that vortex reconnections cause acoustic emission. In quantum fluids, numerical simulations of the GP model show that acoustic emission occurs at every reconnection [29, 30]. The dissipated energy during each reconnection is approximately 3ξ times the vortex line energy per unit length. We can estimate how L decays by this mechanism. The number of reconnection events per volume per time is on the order of $\kappa L^{5/2}$ [27]. Since each reconnection should reduce the vortex length by the order of ξ, the decay of L can be described as $dL/dt = -\chi_1 \xi \kappa L^{5/2}$ with a constant χ_1 of order unity. The solution is

$$\frac{1}{L^{3/2}} = \frac{1}{L_0^{3/2}} + \frac{3}{2}\chi_1 \xi \kappa t. \tag{27}$$

In superfluid helium, especially ^{4}He, ξ is so small that decay due to this mechanism should be negligible.

The second possible mechanism is the radiation of sound (phonons) by the oscillatory motion of a vortex core. The characteristic frequencies of vortex motion on a scale ℓ are of order κ/ℓ^2, which is too small to cause effective radiation [43]. In order to make the radiation effective, the vortices should form small-scale structures, which would be realized by two consecutive processes. The first process is due to vortex reconnections [63]. In a dense isotropic tangle, vortex reconnections occur repeatedly at a rate of order κ/ℓ^5 per unit volume [27]. When two vortices approach one another, they twist so that they become locally antiparallel, and reconnect [12]. They then separate leaving a local small-scale structure. However, even such local structures created by single reconnection events are insufficient to

cause effective acoustic radiation. The next process occurs due to a Kelvin-wave cascade described in Section 7.2. The Kelvin-wave cascade could transfer the energy into the small scales in which the radiation of sound becomes effective.

In actual experiments, we may have to consider the effects of vortex diffusion, even though these effects are not due to dissipation. Using the vortex filament model, Tsubota *et al*. numerically studied how an inhomogeneous vortex tangle diffuses [74]. The obtained diffusion of the line length density $L(\mathbf{x}, t)$ was well described by

$$\frac{dL(\mathbf{x}, t)}{dt} = -\chi \frac{\kappa}{2\pi} L(\mathbf{x}, t)^2 + D\nabla^2 L(\mathbf{x}, t), \tag{28}$$

where χ is a dimensionless constant dependent on temperature. Without the second term on the right-hand side, this is Vinen's equation (25) [9]. The second term represents the diffusion of a vortex tangle. The numerical results show that the diffusion constant D is approximately 0.1κ. The dimensional argument indicates that D must be on the order of κ [74].

6.5 New Experiments on Quantum Turbulence

This subsection reviews briefly recent important experiments on QT, although additional research is needed for all of these experiments.

6.5.1 Temperature-dependent transition to QT

Krusius *et al*. conducted a series of experimental studies on QT in superfluid ^{3}He -B under rotation [75, 76, 77, 78, 79, 80] and observed the strong temperature-dependent transition of a few seed vortices to turbulence. A seed vortex can develop into turbulence when the temperature is lower than the onset temperature T_{on}, whereas the seed vortex does not lead to turbulence above T_{on}. The onset temperature T_{on} is approximately $0.6T_c$ with the superfluid transition temperature T_c being independent of flow velocity[78]. The key characteristics of using ^{3}He -B for research on QT are as follows. First, the normal fluid component is too viscous to become turbulent, which is very different from the case of superfluid ^{4}He. Secondly, monitoring the NMR absorption spectra enables us to count the number of quantized vortices, which is not possible in ^{4}He.

What the experiments revealed is the following. A seed vortex is injected into ^{3}He-B in a cylindrical vessel rotating with the angular velocity Ω. In the laboratory frame, the normal fluid component causes solid body rotation, while the superfluid component remains at rest. When the temperature is higher than T_{on}, the vortex just orientates along the rotational axis because of the mutual friction. If the temperature is lower than T_{on}, however, the vortex becomes unstable, through several vortex reconnections that occur chiefly near the boundary[79], splitting into lots of vortices, and eventually reaching an equilibrium vortex lattice state. While the turbulent front propagates to the vortex-free region, the front takes on the beautiful "twisted vortex state" [80]. The onset temperature is determined by considering the dynamic mutual friction parameter $\zeta = (1 - \alpha')/\alpha$, where α and α' are the mutual friction coefficients appearing in Eq. (7) [75]. This parameter ζ works in this system like the Reynolds number in a usual fluid.

6.5.2 Dissipation at Very Low Temperatures

Recently a few experimental studies on these topics have been conducted, showing the reduction of the dissipation at low temperatures. Eltsov *et al*. studied the vortex front propagation into a region of vortex-free flow in rotating superfluid ^{3}He-B by NMR measurements following a series of investigations [81]. The observed front velocity as a function of temperature shows the transition from laminar through quasiclassical turbulent to quantum turbulent. The front velocity is related to the effective dissipation, which exhibits a peculiar reduction at very low temperatures below approximately $0.25T_c$ with the critical temperature T_c. Eltsov *et al*. claim that this is attributable to the bottleneck effect. Walmsley *et al*. made another observation of the effective viscosity of turbulence in superfluid ^{4}He [44]. Turbulence was produced by an impulsive spin down from an angular velocity to rest for a cube-shaped container, and the line length density was measured by scattering negative ions. The observed effective kinematic viscosity showed the striking reduction at low temperatures below approximately 0.8 K. In this case, the bottleneck effect may not be so significant. The authors believe this may be due to another mechanism, namely, the difficulty in transferring energy through

wavenumbers from the three-dimensional Richardson cascade to the one-dimensional Kelvin-wave cascade.

6.5.3 Quantum turbulence created by vibrating structures

Recently, vibrating structures including discs, spheres, grids, and wires, have been used for research into QT [49]. Despite differences between the structures, the experiments show surprisingly similar behavior. When a classical viscous fluid steadily flows past a structure, the flow changes from laminar to turbulence in the wake as the Reynolds number increases. The net drag force on the structure is often expressed in terms of the drag coefficient C_D as $F_D = 1/2 C_D \rho A \upsilon^2$, where A is the projected area of the structure onto a plane normal to the flow. For laminar viscous flow, the drag is approximately proportional to υ so that $C_D \sim \upsilon^{-1}$, while turbulent flow with high Reynolds number yields a drag coefficient C_D of order unity. This drastic reduction in the drag force is called the drag crisis, and is closely related to the formation of the boundary layer [82]. A boundary layer in a high velocity gradient produces eddies. However, such boundary layers do not appear in the superfluid component. Another classical aspect is the effect of oscillations. The oscillatory case is more complicated than that of steady flow because a second length scale appears in addition to the linear size of the structure, namely the viscous penetration depth $\delta = \sqrt{2\nu/\omega}$ where ω is the oscillation frequency of the structure [49]. Owing to the importance of the topic in marine engineering, a number of experimental studies have been published on oscillatory classical flow past a cylinder. As laminar flow becomes unstable, the drag coefficient C_D reduces to a value of order unity. However, the values of C_D oscillate within the range 0.5 to 2.0, showing a more complicated transition to turbulence than in the case of steady flow. Visual observations show that vortices are formed in the wake of the oscillating cylinder. A few experimental studies have reported classical flow around an oscillating sphere. A typical experiment shows that a single vortex ring is generated and shed during each half period of oscillation [83].

Typical behavior appeared in the pioneering observation of QT for an oscillating microsphere in superfluid ^{4}He by Jäger *et al*. [84]. The sphere they used had a radius of approximately 100 μm. It was made from a strongly ferromagnetic material and was magnetically levitated in superfluid ^{4}He. Its response to an alternating drive was observed. At low drives, the velocity response υ was proportional to the drive F_D, taking the "laminar" form $F_D = \lambda(T)\upsilon$ with a temperature-dependent coefficient $\lambda(T)$. At high drives, the response changed to the "turbulent" form $F_D = \gamma(T)(\upsilon^2 - \upsilon_2^0)$ above a critical velocity υ_0. At low temperatures, the transition from laminar to turbulent response was accompanied by hysteresis. Subsequently, several groups have experimentally investigated the transition to turbulence in superfluid ^{4}He and ^{3}He-B by using grids, wires, and tuning forks [49].

These experimental studies reported some common behaviors independent of the details of the structures, including its type, shape, and surface roughness. The observed critical velocities were in the range from 1 to 200 mm/s. Since the velocity was lower than the Landau critical velocity of approximately 50 m/s [3], the transition to turbulence should come not from intrinsic nucleation of vortices but from extension or amplification of remnant vortices.[7] Such behavior is seen in the numerical simulation using the vortex filament model [86]. Figure 7 shows how the remnant vortices initially attached to a sphere develop into turbulence under an oscillating flow. Many unresolved problems remain, such as the nature of the critical velocity and the origin of the hysteresis in the transition between the laminar and turbulent response.

6.5.4 Visualization of QT

There has been little direct experimental information about flow in superfluid ^{4}He because standard flow visualization techniques are not applicable to it. However, the situation is changing [50]. For QT, one can seed the fluid with tracer particles in order to visualize the flow field. Quantized vortices are observable by appropriate optical techniques.

A significant contribution was made by Zhang and Van Sciver [87]. Using the particle image velocimetry (PIV) technique with 1.7-μm-diameter polymer particles, they visualized a large-scale turbulent flow both in front of and behind a cylinder in counterflowing superfluid ^{4}He at finite temperatures. In classical fluids, such turbulent structures are seen downstream of objects such as cylinders, and the structures periodically detach to form a vortex sheet. In the case of ^{4}He

[7]Superfluid ^{4}He at rest usually contains remnant vortices [85]. They are metastably pinned between the walls of the container and are established when the liquid is cooled down through the λ point to the superfluid phase.

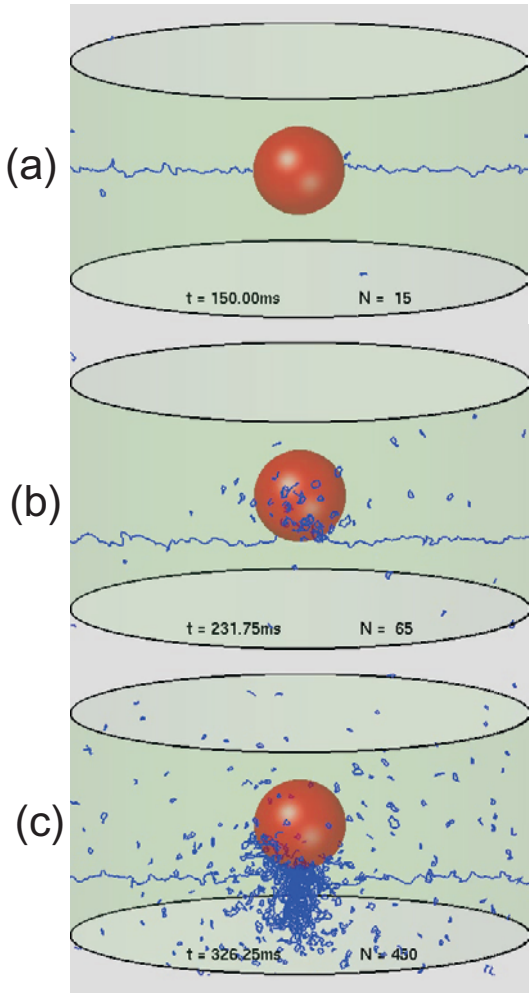

Fig. 7. Evolution of a vortex line near a sphere of radius 100 μm in an oscillating superflow of 150 mm/s at 200 Hz. [Hänninen, Tsubota, and Vinen, Phys. Rev. B **75** (2007) 064502, reproduced with permission. Copyright 2007 by the American Physical Society.]

counterflow, however, the locations of the large-scale turbulent structures were relatively stable; they did not detach and move downstream, although local fluctuations in the turbulence were evident.

Do the tracer particles follow the normal flow, the superflow, or a more complex flow?

Barenghi *et al*. studied this question theoretically and numerically to show that the situation changes depending on the size and mass of the tracer particles [88, 89, 90].

Another important contribution was the visualization of quantized vortices by Bewley *et al*. [91]. In their experiments, liquid helium was seeded with solid hydrogen particles smaller than 2.7 μm in diameter at a temperature slightly above T_λ, following which the fluid was cooled to below T_λ. When the temperature is above T_λ, a homogeneous cloud of the particles was seen that disperses throughout the fluid. However, on passing through T_λ, the particles coalesced into web-like structures. Bewley *et al*. suggested that these structures represent decorated quantized vortex lines. They reported that the vortex lines form connections rather than remaining separated, and were homogeneously distributed throughout the fluid. The observed fork-like structures may indicate that several vortices are attached to the same particle. Applying this technique to thermal counter flow, Paoletti *et al*. have directly visualized the two-fluid behavior [92].

7. QUANTUM TURBULENCE IN ATOMIC BECs

The long history of research into superfluid helium has uncovered two main cooperative phenomena of quantized vortices: vortex lattices under rotation and vortex tangles in QT. However, almost all studies of quantized vortices in atomic BECs have been limited to vortex lattices. This section briefly discusses QT in atomic BECs.

Kobayashi and Tsubota proposed an easy, powerful method to make a steady QT in a trapped BEC, by using precession [93]. The dynamics of the wavefunction are described by the GP equation with dissipation. First, one traps a BEC cloud in a weakly elliptical harmonic potential,

$$U(\mathbf{r}) = \frac{m\omega^2}{2}\left[(1-\delta_1)(1-\delta_2)x^2 + (1+\delta_1)(1-\delta_2)y^2 + (1-\delta_2)z^2\right], \tag{29}$$

where the parameters δ_1 and δ_2 exhibit elliptical deformation in the xy- and zx-planes. Second, to transform the BEC into a turbulent state, a rotation is applied along the z-axis followed by a rotation along the x -axis, as shown in Fig. 8(a). The rotation vector is $\Omega(t) = (\Omega_x, \Omega_z \sin\Omega_x t, \Omega_z \cos \Omega_x t)$ where Ω_z and Ω_x are the frequencies of the first and second rotations, respectively. Consider the case where the spinning and precessing rotational axes are perpendicular to each other. Then the two rotations do not commute and cannot be represented by their sum. This form of precession is also used for turbulence in water [94].

Starting from a stationary solution without rotation or elliptical deformation, Kobayashi *et al.* numerically calculated the time development of the GP equation by turning on the rotation $\Omega_x = \Omega_z = 0.6$ and elliptical deformation $\delta_1 = \delta_2 = 0.025$. By monitoring the kinetic energy and anisotropic parameters, the system eventually becomes statistically steady and isotropic. In the steady state, the spectrum $E^i_{kin}(k, t)$ of the incompressible kinetic energy per unit mass is consistent with the Kolmogorov law [Fig. 8(b)]. The inertial range which sustains the Kolmogorov law is determined by the Thomas-Fermi radius R_{TF} and the coherence length ξ. The application of a combined precession around three axes enables one to obtain more isotropic QT [95]. The velocity field in a BEC cloud can be observed by Bragg spectroscopy [96], enabling one to obtain the energy spectrum.

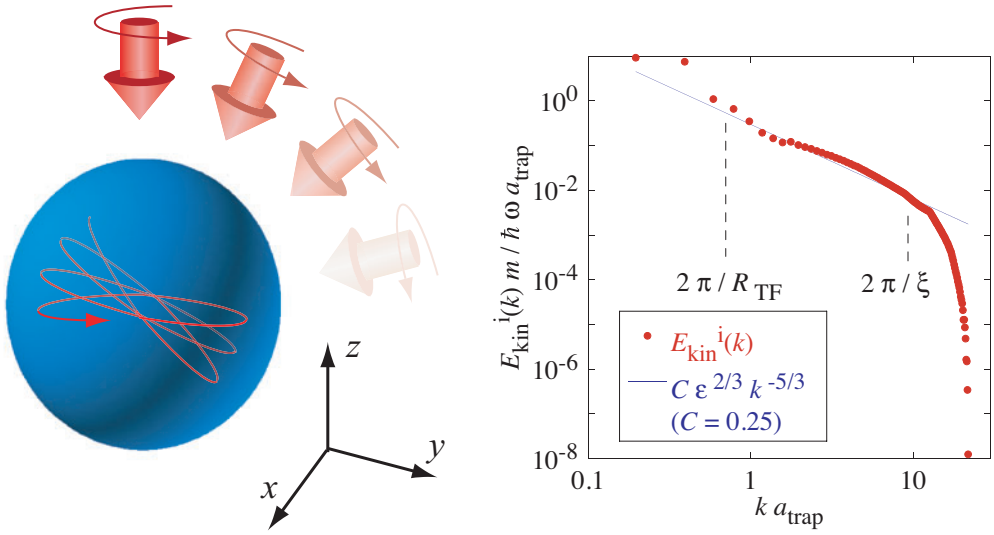

Fig. 8. QT in atomic BECs [21]. (a) The BEC cloud is subject to precessions. (b) Energy spectrum of a steady QT. The dots are a numerically obtained spectrum of the incompressible kinetic energy, while the solid line is the Kolmogorov spectrum. Here, R_{TF} is the Thomas-Fermi radius amd $a_{trap} = \sqrt{\hbar/m\omega}$ is the characteristic length scale of the trap.

There are several advantages of studying QT in atomic BECs compared to in superfluid helium. First, one can observe the vortex configuration, probably even the Richardson cascade process of vortices. In fact one can directly study the relation between the real-space Richardson cascade and the wavenumber-space cascade (the Kolmogorov spectrum). Second, one can control the transition to turbulence by changing the rotational frequencies or other parameters. For example, rotation along one axis forms a vortex lattice. If one applies another rotation, it may rotate the lattice if the frequency is low. If the frequency is high, however, the second rotation can melt the lattice into a vortex tangle. That would enable one to investigate in detail the entire transition to turbulence. Third, by changing the

shape of the trapping potential, one can study the effect of the anisotropy on turbulence; a typical question is how the Kolmogorov spectrum is changed when the BEC becomes anisotropic. This issue is related to the transition between 2D and 3D turbulence. Fourth, one can create rich QT in multicomponent BECs by controlling the interaction parameters. Multicomponent BECs have been extensively studied and found to create many kinds of vortex structures depending on the intercomponent interaction [97]. By using such systems, we will be able to make multicomponent QT coupled through the interaction.

8. CONCLUSIONS

In this article, we have reviewed recent research on quantum hydrodynamics and turbulence in superfluid helium and atomic BECs. Quantum turbulence has been long studied in superfluid helium, while it is realized experimentally in atomic BECs too very lately [98]. Research on QT is currently one of the most important branches in low-temperature physics, attracting the attention of many scientists. QT is comprised of quantized vortices as definite elements, which differs greatly from conventional turbulence. Thus, investigation of QT may lead to a breakthrough in understanding one of the great mysteries of nature since the era of da Vinci. There are many related topics not addressed in this article, regarding which we refer the readers to other review articles [19, 20].

ACKNOWLEDGMENT

The author thanks Kenichi Kasamatsu and Michikazu Kobayashi for help with the manuscript. The author acknowledges a Grant-in-Aid for Scientific Research from JSPS (Grant No. 18340109) and a Grant-in-Aid for Scientific Research on Priority Areas from MEXT (Grant No. 17071008).

REFERENCES

[1] Feynman, R.P., Leighton R.B., and Sands M., *The Feynman Lectures on Physics*, Addison-Wesley, San Francisco, 2006.

[2] Pethick, C. J. and Smith, H., *Bose-Einstein Condensation in Dilute Gases*, Cambridge University Press, Cambridge, 2002.

[3] Tilley, D. R. and Tilley, J., *Superfluidity and Superconductivity*, 3rd edn., Institute of Physics Publishing, Bristol and Philadelphia, 1990.

[4] Feynman, R. P., Application of quantum mechanics to liquid helium, in: Gorter, C. J., ed., *Prog. Low Temp. Phys.*, North-Holland, Amsterdam, 1955, Vol. I, 17–53.

[5] Vinen, W. F., The detection of a single quantum of circulation in liquid helium II, *Proc. Roy. Soc. A*, 1958, 260, 400–413.

[6] Gorter, C. J. and Mellink, J. H., On the irreversible processes in liquid helium II, *Physica*, 1949, 15, 285–304.

[7] Vinen, W. F., Mutual friction in a heat current in liquid helium II: I. Experiments on steady heat currents, *Proc. Roy. Soc. A*, 1957, 240, 114–127.

[8] Vinen, W. F., Mutual friction in a heat current in liquid helium II: II. Experiments on transient effects, *Proc. Roy. Soc. A*, 1957, 240, 128–143.

[9] Vinen, W. F., Mutual friction in a heat current in liquid helium II: III. Theory of the mutual friction, *Proc . Roy. Soc. A* , 1957, 242, 493–515.

[10] Vinen, W. F., Mutual friction in a heat current in liquid helium II: IV. Critical heat currents in wide channels, *Proc. Roy. Soc. A*, 1958, 243, 400–413.

[11] Tough, J. T., Superfluid turbulence, in: Gorter, C. J., ed., *Prog. Low Temp. Phys.*, North-Holland, Amsterdam, 1982, Vol. VIII, 133–220.

[12] Schwarz, K.W., Three-dimensional vortex dynamics in superfluid 4He: Line-line and line-boundary interactions, *Phys. Rev. B*, 1985, 31, 5782–5803.

[13] Schwarz, K. W., Three-dimensional vortex dynamics in superfluid 4He: Homogenous superfluid turbulence, *Phys. Rev. B*, 1988, 38, 2398–2417.

[14] Frisch, U., *Turbulence*, Cambridge University Press, Cambridge, 1995.

[15] Kolmogorov, A. N., The local structure of turbulence in incompressible viscous fluid for very large Reynolds number, *Dokl. Akad. Nauk SSSR*, 1941, 30, 299–303 [reprinted in *Proc. Roy. Soc. A*, 1991, 434, 9–13].

[16] Kolmogorov, A. N., On degeneration (decay) of isotropic turbulence in an incompressible viscous liquid, *Dokl. Akad. Nauk SSSR*, 1941, 31, 538–540 [reprinted in *Proc. Roy. Soc. A*, 1991, 434, 15–17].

[17] Vinen, W. F. and Niemela, J. J., Quantum turbulence, *J. Low Temp. Phys.*, 2002, 128, 167–231.

[18] Vinen, W. F., An introduction to quantum turbulence, *J. Low Temp. Phys.*, 2006, 145, 7–24.

[19] Halperin, W. P. and Tsubota, M., ed., *Prog. Low Temp. Phys.*, Elsevier, Amsterdam, 2008, Vol. 16.

[20] Tsubota, M., Quantum turbulence, *J. Phys. Soc. Jpn.*, 2008, 78, 111006.

[21] Tsubota, M., Quantum turbulence, Contemporary Physics, 2009, 50, 463-475.

[22] Kasamatsu, K. and Tsubota, M., Quantized vortices in atomic Bose-Einstein condensates, in: Halperin, W. P. and Tsubota, M., ed., *Prog. Low Temp. Phys.*, Elsevier, Amsterdam, 2008, Vol.16, 351–403.

[23] Abo-Shaeer, J. R., Raman, C., Vogels, M. and Ketterle, W., Observation of vortex lattices in Bose-Einstein condensates, *Science*, 2001, 292, 476–479.

[24] Madison, K. W., Chevy, F., Wlhlleben, W. and Dalibard, J., Vortex formation in a stirred Bose-Einstein condensate, *Phys. Rev. Lett.*, 2000, 84, 806–809.

[25] Madison, K. W., Chevy, F., Wlhlleben, W. and Dalibard, J, Statonary states of a rotating Bose-Einstein condensate: Routes to vortex nucleation, *Phys. Rev. Lett.*, 2001, 86, 4443–4446.

[26] Saffman P. G., *Vortex Dynamics*, Cambridge University Press, Cambridge, 1992.

[27] Tsubota, M., Araki, T. and Nemirovskii, S. K., Dynamics of vortex tangle without mutual friction in superfluid ^{4}He, *Phys. Rev. B*, 2000, 62, 11751–11762.

[28] Koplik, J. and Levine, H., Vortex reconnection in superfluid helium, *Phys. Rev. Lett.*, 1993, 71, 1375–1378.

[29] Leadbeater, M., Winiecki, T., Samuels, D. C., Barenghi, C. F. and Adams, C. S., Sound emission due to superfluid vortex reconnections, *Phys. Rev. Lett.*, 2001, 86, 1410–1413.

[30] Ogawa, S., Tsubota, M. and Hattori, Y., Study of reconnection and acoustic emission of quantized vortices in superfluid by the numerical analysis of the Gross-Pitaevskii equation, *J. Phys. Soc. Jpn.*, 2002, 71, 813–821.

[31] Williams, G.A. and Packard, R. E., Photographs of quantized vortex lines in rotating He II, *Phys. Rev. Lett.*, 1974, 33, 280–283.

[32] Yarmchuck, E. J. and Packard, R. E., Photographic studies of quantized vortex lines, *J. Low Temp. Phys.*, 1982, 46, 479–515.

[33] Matthews, M. R., Anderson, B. P., Haljan, P. C., Hall, D. S., Wieman, C. E. and Cornell, E. A., Vortices in a Bose-Einstein condensate, *Phys. Rev. Lett.*, 1999, 83, 2498–2501.

[34] Tsubota, M., Kasamatsu, K. and Ueda, M., Vortex lattice formation in a rotating Bose-Einstein condensate, *Phys. Rev. A*, 202, 65, 023603.

[35] Kasamatsu, K., Tsubota M. and Ueda M., Nonlinear dynamics of vortex lattice formation in a rotating Bose-Einstein condensate, *Phys. Rev. A*, 2003, 67, 033610.

[36] Kasamatsu, K., Machida, M., Sasa, N. and Tsubota, M., Three-dimensional dynamics of vortex-lattice formation in Bose-Einstein condensate, *Phys. Rev. A*, 2005, 71, 063616.

[37] Maurer, J. and Tabeling, P., Local investigation of superfluid turbulence, *Europhys. Lett.*, 1998, 43, 29–34.

[38] Stalp, S. R., Skrbek, L. and Donnelly, R. J., Decay of grid turbulence in a finite channel, *Phys. Rev. Lett.*, 1999, 82, 4831–4834.

[39] Skrbek, L., Niemela, J. J. and Donnelly, R. J., Four regimes of decaying grid turbulence in a finite channel, *Phys. Rev. Lett.*, 2000, 85, 2973–2976.

[40] Skrbek, L. and Stalp, S. R., On the decay of homogeneous isotropic turbulence, *Phys. Fluids*, 1997, 12, 1997–2019.

[41] Stalp, S. R., Niemela, J. J., Vinen, W. F. and Donnelly, R. J., Dissipation of grid turbulence in helium II, *Phys. Fluids*, 2002, 14, 1377–1379.

[42] Hinze, J. O., *Turbulence* , 2nd edn., McGraw Hill, New York, 1975.

[43] Vinen, W. F., Classical character of turbulence in a quantum liquid, *Phys. Rev. B*, 2000, 61, 1410–1420.

[44] Walmsley, P. M., Golov, A. I., Hall, H. E., Levchenko, A. A. and Vinen, W. F., Dissipation of

quantum turbulence in the zero temperature limit, *Phys. Rev. Lett.*, 2007, 99, 265302.

[45] Bradley, D. I., Clubb, D. O., Fisher, S. N., Guenault, A. M., Halay, R. P., Matthews, C. J., Pickett, G. R., Tsepelin, V. and Zaki, K., Decay of pure quantum turbulence in superfluid ^{3}He-B, *Phys. Rev. Lett.*, 2006, 96, 035301.

[46] Fisher, S. N. and Pickett, G. R., Quantized turbulence in superfluid ^{3}He at very low temperatures, in: Halperin, W. P. and Tsubota, M., ed., *Prog. Low Temp. Phys.*, Elsevier, Amsterdam, 2008, Vol. 16, 147–194.

[47] L'vov, V. S., Nazarenko, S. V. and Skrbek, L., Energy spectra of developed turbulence in helium superfluids, *J. Low Temp. Phys.*, 2006, 145, 125–142.

[48] Tsubota, M. and Kobayashi, M., Energy spectra of quantum turbulence, in: Halperin, W. P. and Tsubota, M., ed., *Prog. Low Temp. Phys.*, Elsevier, Amsterdam, 2008, Vol. 16, 1–43.

[49] Skrbek, L. and Vinen, W. F., The use of vibrating structures in the study of quantum turbulence, in: Halperin, W. P. and Tsubota, M., ed., *Prog. Low Temp. Phys.*, Elsevier, Amsterdam, 2008, Vol. 16, 195–246.

[50] Van Sciver, S. W. and Barenghi, C. F., Visualization of quantum turbulence, in: Halperin, W. P. and Tsubota, M., ed., *Prog. Low Temp. Phys.*, Elsevier, Amsterdam, 2008, Vol. 16, 247–304.

[51] Nore, C., Abid, M. and Brachet, M. E., Kolmogorov turbulence in low-temperature superflows, *Phys. Rev. Lett.*, 1997, 78, 3296–3299.

[52] Nore, C., Abid, M. and Brachet, M. E., Decaying Kolmogorov turbulence in a model of superflow, *Phys. Fluids*, 1997, 9, 2644–2669.

[53] Araki, T., Tsubota, M. and Nemirovskii, S. K., Energy spectrum of superfluid turbulence with no normal-fluid component, *Phys. Rev. Lett.*, 2002, 89, 145301.

[54] Kobayashi, M. and Tsubota, M., Kolmogorov spectrum of superfluid turbulence: Numerical analysis of the Gross-Pitaevskii equation with a small-scale dissipation, *Phys. Rev. Lett.*, 2005, 94, 065302.

[55] Kobayashi, M. and Tsubota, M., Kolmogorov spectrum of quantum turbulence, *J. Phys. Soc. Jpn.*, 2005, 74, 3248–3258.

[56] Kobayashi, M. and Tsubota, M., Thermal dissipation in quantum turbulence, *Phys. Rev. Lett.*, 2006, 97, 145301.

[57] Kobayashi, M. and Tsubota, M., Decay of quantized vortices in quantum turbulence, *J. Low Temp. Phys.*, 2006, 145, 209–218.

[58] Thomson, J., Vibrations of a columnar vortex, *Phil Mag.*, 1880, 10, 155–168.

[59] Hall, H. E., An experimental and theoretical study of torsional oscillations in uniformly rotating liquid helium II, *Proc. Roy. Soc. London A*, 1958, 245, 546–561.

[60] Hall, H. E., The rotation of helium II, *Phil. Mag. Suppl.*, 1960, 9, 89–146.

[61] Vinen, W. F., Decay of superfluid turbulence at a very low temperature: The radiation of sound from a Kelvin wave on a quantized vortex, *Phys. Rev. B*, 2001, 64, 134520.

[62] Samuels, D. C. and Donnelly, R. J., Sideband instability and recurrence of Kelvin waves on vortex cores, *Phys. Rev. Lett.*, 1990, 64, 1385–1388.

[63] Svistunov, B. V., Superfluid turbulence in the low-temperature limit, *Phys. Rev. B*, 1995, 52, 3647–3653.

[64] Kivotides, D., Vassilicos, J. C., Samuels, D. C. and Barenghi, C. F., Kelvin waves cascade in superfluid turbulence, *Phys. Rev. Lett.*, 2001, 86, 3080–3083.

[65] Vinen, W. F., Tsubota, M. and Mitani, A., Kelvin-wave cascade on a vortex in superfluid 4He at a very low temperature, *Phys. Rev. Lett.*, 2003, 91,135301.

[66] Kozik, E. and Svistunov, B. V., Kelvin-wave cascade and decay of superfluid turbulence, *Phys. Rev. Lett.*, 2004, 92, 035301.

[67] Kozik, E. and Svistunov, B. V., Scale-separation scheme for simulating superfluid turbulence: Kelvin-wave cascade, *Phys. Rev. Lett.*, 2005, 94, 025301.

[68] Kozik, E. and Svistunov, B. V., Vortex-phonon interaction, *Phys. Rev. B*, 2005, 72, 172505.

[69] L'vov, V. S., Nazarenko, S. V. and Rudenko, O., Bottleneck crossover between classical and

quantum superfluid turbulence, *Phys. Rev. B*, 2007, 76, 024520.

[70] Kozik, E. and Svistunov, B. V., Kolmogorov and Kelvin-wave cascades of superfluid turbulence at T = 0: What lies between, *Phys. Rev. B*, 2008, 77, 060502.

[71] Kozik, E. and Svistunov, B. V., Scanning superfluid-turbulence cascade by its low-temperature cutoff, *Phys. Rev. Lett.*, 2008, 100, 195302.

[72] Cannaughtoni, C. and Nazarenko, S. V., Warm cascades and anomalous scaling in a diffusion model of turbulence, *Phys. Rev. Lett*, 2004, 92, 044501.

[73] Walmsley, P. M. and Golov, A. I., Quantum and quasiclassical types of superfluid turbulence, *Phys. Rev. Lett.*, 2008, 100, 245301.

[74] Tsubota, M., Araki T. and Vinen, W. F., Diffusion of an inhomogeneous vortex tangle, *Physica B*, 2003, 329–333, 224–225.

[75] Finne, A. P., Eltsov, V. B., Hänninen, R., Kopnin, N. B., Kopu, J., Krusius, M., Tsubota, M. and Volovik, G. E., Dynamics of vortices and interfaces in superfluid ^{3}He, *Rep. Progr. Phys.*, 2006, 69, 3157–3230.

[76] Eltsov, V. B., de Graaf, R., Hänninen, R., Krusius, K., Solntsev, R. E, L'vov, V. S., Golov, A. I. and Walmsley, P. M., Turbulent dynamics in rotating helium superfluids, in: Halperin, W. P. and Tsubota, M., ed., *Prog. Low Temp. Phys.*, Elsevier, Amsterdam, 2008, Vol. 16, 45–146.

[77] Finne, A. P., Araki, T., Blaauwgeers, R., Eltsov, V. B., Kopnin, N. B., Krusius, M., Skrbek, L., Tsubota, M. and Volovik, G. E., An intrinsic velocity-independent criterion for superfluid turbulence, *Nature*, 2003, 424, 1022–1025.

[78] Finne, A. P., Boldarev, R., Eltsov, V. B. and Krusius, M., Measurement of turbulence in superfluid ^{3}He-B, *J. Low Temp. Phys.*, 2004, 136, 249–279.

[79] Finne, A. P., Eltsov, V. B., Eska, G., Hänninen, R., Kopu, J., Krusius, M., Thuneberg, E. V. and Tsubota, M., Vortex multiplication in applied flow: a precursor to superfluid turbulence, *Phys. Rev. Lett.*, 2006, 96, 085301.

[80] Eltsov, V. B., Finne, A. P., Hänninen, R., Kopu, J., Krusius, M., Tsubota, M. and Thuneberg, E. V., Twisted vortex state, *Phys. Rev. Lett.*, 2006, 96, 215302.

[81] Eltsov, V. B., Golov, A. I., de Graaf, R., Hänninen, R., Krusius, M., L'vov, V. S. and Solntsev, R. E., Quantum turbulence in a propagating superfluid vortex front, *Phys. Rev. Lett.*, 2007, 99, 265301.

[82] Landau, L. D. and Lifshitz, E. M., *Fluid mechanics*, 2nd edn., Pergamon Press, Oxford, 1987.

[83] Donnelly, R. J., private communication.

[84] Jäger, J., Schuderer, B. and Schoepe, W., Turbulent and laminar drag of superfluid helium on an oscillating microsphere, *Phys. Rev. Lett.*, 1995, 74, 566–569.

[85] Awschalom, D. D. and Schwarz, K. W., Observation of a remanent vorte-line density in superfluid helium, *Phys. Rev. Lett.*, 1984, 52, 49–52.

[86] Hänninen, R., Tsubota, M. and Vinen, W. F., Generation of turbulence by oscillating structures in superfluid helium at very low temperatures, *Phys. Rev. B*, 2007, 75, 064502.

[87] Zhang, T. and Van Sciver, S. W., Large-scale turbulent flow around a cylinder in counterfow superfluid ^{4}He (He(II)), *Nature Phys.*, 2005, 1, 36–38.

[88] Poole, D. R., Barenghi, C. F., Sergeev, Y. A. and Vinen, W. F., Motion of tracer particles in He II, *Phys. Rev. B*, 2005, 71, 064514.

[89] Kivotides, D., Barenghi, C. F. and Sergeev, Y. A., Collision of a tracer particle and a quantized vortex in superfluid helium: Self-consistent calculations, *Phys. Rev. B*, 2007, 75, 212502.

[90] Kivotides, D., Barenghi, C. F. and Sergeev, Y. A., Interactions between particles and quantized vortices in superfluid helium, *Phys. Rev. B*, 2008, 014527.

[91] Bewley, G. P., Lathrop, D. P. and Sreenivasan, K. R., Visualization of quantized vortices, *Nature*, 2006, 441, 588.

[92] Paelotti, M. S., Firrito, R. B., Sreenivasan, K. R. and Lathrop, D. P., Visualization of superfluid helium flow, *J. Phys. Soc. Jpn.*, 2008, 77, 111007.

[93] Kobayashi, M. and Tsubota, M., Quantum turbulence in a trapped Bose-Einstein condensate, *Phys. Rev. A*, 2007, 76, 045603.

[94] Goto, S., Ishii, N., Kida, S. and Nishioka, M., Turbulence generator using a precessing sphere,

Phys. *Fluids*, 2007, 19, 061705.

[95] Kobayashi, M. and Tsubota, M., Quantum turbulence in a trapped Bose-Einstein condensate under combined rotations around three axes, *J*. *Low Temp*. *Phys*., 2008, 150, (2008), 587–592.

[96] Stenger, J., Inouye, S., Chikkatur, A. P., Stamper-Kurn, D. M., Pritchard, D. E. and Ketterle, W., Bragg spectroscopy of a Bose-Einstein condensate, *Phys*. *Rev*. *Lett*., 1999, 82, 4569–4573.

[97] Kasamatsu, K., Tsubota, M. and Ueda, M., Vortices in multicomponent Bose-Einstein condensates, *Int*. *J*. *Mod*. *Phys*. *B*, 2005, 19, 1835–1904.

[98] Henn, E. A. L., Seman, J. A., Roati, G., Magalhaes, K. M. F. and Bagnato, V. S., Emergence of turbulence in an oscillating Bose-Einstein condensate, *Phys*. *Rev*. *Lett*., 2009, 103, 045301.